Computer Simulation on Interaction of the Solar Wind with Jovian and Kronian Magnetospheres

Keiichiro FUKAZAWA

Abstract

Both Jupiter and Saturn have similar characters such as rapid rotation, the moon providing plasmas into the magnetosphere and giant body. The major difference is the magnitude of the intrinsic magnetic field. Due to these characteristics Jupiter and Saturn are often compared each other. In this dissertation, we study the dynamics of the Jovian magnetosphere and that of the Kronian magnetosphere.

It has long been recognized that the solar wind and interplanetary magnetic field (IMF) control magnetospheric dynamics at the Earth. On the other hand, a massive rotating equatorial plasma sheet dominates the Jovian magnetosphere, and the solar wind and the IMF are not thought to be as important as at Earth. However, in our following simulation study, we found that for a purely northward IMF the Jovian magnetosphere reached an unsteady state in which a nearly periodic series of magnetic X and O lines are launched tailward.

In this study we have carried out a series of three-dimensional global magnetohydrodynamic (MHD) simulations to investigate the causes of dynamic behavior of the Jovian magnetosphere. Both the effects of changes in the solar wind dynamic pressure and IMF are considered. First, the effects of dynamic pressure on the magnetospheric configuration are examined in the absence of IMF by calculating the magnetospheric configuration for four levels of solar wind dynamic pressure. The simulation started by setting the pressure to 0.090 nPa and ran the code until a quasi-steady magnetosphere

resulted. Then the pressure decreased three times until it reached 0.011 nPa. In the all simulations we ran the code until a quasi-steady magnetosphere resulted.

Next we simulate the magnetosphere for northward and southward IMF starting from the configuration with 0.011 nPa. Starting from the simulation with southward IMF, a series of northward IMF simulations were examined in which both the IMF magnitude and dynamic pressure were varied.

When B_z was 0.105 nT and the pressure was 0.011 nPa, X/O pairs were launched tailward with an average period of 34.3 hours. For a fixed B_z of 0.105 nT the period increased with increasing dynamic pressure until at 0.045 nPa when the tail settled into a steadily reconnecting configuration. For a fixed dynamic pressure of 0.090 nPa and B_z = 0.420 nT the X/O pairs formed with two periods (~20 hours and ~50 hours) while the reconnection again became steady when the IMF was reduced to 0.105 nT. Thus higher dynamic pressure makes the period of plasmoid ejection longer while increasing northward IMF makes the period shorter. This behavior can be understood by noting that the solar wind dynamic pressure controls the location of the rotation dominated region while the IMF controls the location of the tail X-line. When the tail X-line is near the outer boundary of the rotation dominated region, the injected flux from the neutral line can rotate around Jupiter and contribute to the reconnection occurring multiple times.

Saturn was thought to have aspects similar to both Jupiter and the Earth with internally driven and solar wind driven dynamics. Recently before arriving at Saturn, Cassini spacecraft observed the upstream solar wind conditions of Saturn and simultaneously Hubble Space Terrescope (HST) observed the aurora of Saturn. As the results of these observations, two explanations have been reported. One is that the Saturn's aurorae is controlled by the solar wind dynamic pressure, another is that the IMF direction is more important than the dynamic pressure on the aurora emission. To in-

vestigate the influence of the IMF on Kronian magnetosphere and aurora brightness, we have used three dimensional MHD simulations. The magnetosphere for three cases with no IMF, northward and southward IMFs were modeled. For all of the simulations the solar wind dynamic pressure was set to the average value at Saturn's orbit.

The subsolar magnetopause and bow shock are insensitive to changes in IMF. In the Y-direction the boundaries are farthest from Saturn for the case without IMF and farther for southward IMF than northward IMF. Flow vortices formed in the magnetotail for all three cases. They were confined to the inner magnetotail for northward IMF but were found throughout the tail for the southward and no IMF cases. For the no IMF the vortices were generated in the morning sector where the rotating Kronian flows were opposite to the solar wind induced flows. For southward IMF the vorticity results from the interaction of flow driven by high latitude reconnection and corotation. For northward IMF vortices were generated in the early morning and evening where the flows from reconnection in Saturn's tail were opposite to the solar wind induced flow.

We used the energy flux toward the ionosphere and upward field-aligned currents as a proxy for diffuse and discrete auroral emissions respectively. For the no IMF case the energy flux is largest in the morning sector poleward of 75^o latitude consistent with HST observations during January 2004. With southward IMF the distribution of energy flux becomes more symmetric than that of no and northward IMF cases. The energy flux in the polar cusp depends on IMF orientation with larger energy flux for northward IMF. Strong upward field-aligned currents extend to the morning sector when the IMF is northward. The strongest field-aligned currents are generated in the flow vortices.

Acknowledgements

I would like to thank my research advisor, Professor Tatsuki Ogino, for his academic and fund support of the research performed in this dissertation. I have benefited greatly from his guidance and attended many workshops and meetings. I would also like to thank Professor Raymond J. Walker for his help and advice. I am deeply grateful for his support of my papers and his kindness at my stay in UCLA/IGPP.

I am also grateful to the 21st Century Center of Excellence (COE) program, "Information Nano-Devices Based on Advanced Plasma Science" and its leader Professor Hideo Sugai for the assistance of my internship to UCLA/IGPP and of my attending the oversea meetings.

I would like to thank Professor Tadahiko Ogawa, Professor Masayoshi Kojima, Dr, Nozomu Nishitani and Dr. Tomoo Nagahama for their assistance in evaluating this dissertation.

I would also like to thank Dr. Kazuo Shiokawa, and Dr. Yuichi Otsuka for their useful comments. Dr. Takayuki Umeda advised me how to go on the doctoral course life and taught me the literacy of researcher. Dr. Yoshizumi Miyoshi gave me the academic and useful comments for Jupiter. Dr. Ryuho Kataoka assisted this dissertation and also advised whole magnetospheric physics to me. Ms. Tomoko Ida, Ms. Kazuko Kondo and Ms. Tomoko Katsuta helped me about life in STEL. I would like to thank all STEL staffs.

Mr. Nobuki Kotake and Mr. Shin Suzuki studied and play together with me in my STEL time. There happened to be many interesting events among us. Thanks to Mr. Shin Tanaka's questions to me, I grew understanding of the simulation. Mr. Shunichi Ogi assisted my simulations. Ms. Chihiro Tao made my thought of Jupiter's magnetospheric dynamics develop. I would like to thank all the students in STEL, in particular Mr. Tomoharu Aoyama, Mr. Juntaro Kondo, Mr. Akimitsu Nakajima, Ms. Kaori Sakaguchi and Mr. Yamashita.

Contents

Chapter 1

Introduction

1.1 Configuration and Dynamics of the Jovian Magnetosphere

Jupiter's magnetospheric configuration is determined by a combination of the solar wind, rapid atmospherically driven rotation, a huge magnetic field which has the opposite direction to Earth's one, and plasma from the moon Io while the overall configuration and dynamics of the Earth's magnetosphere are largely controlled by the solar wind and interplanetary magnetic field (IMF). The Jupiter's dayside magnetosphere contains three distinct regions [*Smith et al.,* 1976]. We describe these regions in Figure 1.1. Near the planet the magnetic field is dipole-like and filled with nearly corotating plasma whose origin is the moon Io. As Iogenic plasma moves outward to populate the magnetosphere, its azimuthal velocity falls below corotation by the conservation of angular momentum. This is offset by a frictional torque in the ionosphere that is communicated to the magnetosphere by field-aligned currents which close in radially outward equatorial currents (**J**) [*Hill*, 1979; 2001; *Vasyliunas*, 1983]. The **J**×**B** force associated with this radial current accelerates the magnetospheric plasma toward

corotation. In the middle magnetosphere the flow subcorotates and the magnetic field becomes highly stretched. In the outer magnetosphere the magnetic field becomes highly variable and the average magnetic field again becomes more dipole-like [*Smith et al.*, 1976]. This outer region is frequently called the "cushion region". Finally, on the night side the middle magnetosphere current sheet merges with the magnetotail current system (see Figure 1.1.).

Vasyliunas [1983] noted that the outward moving flux tubes in the outer current sheet are confined on the dayside by the solar wind, but when they rotate onto the

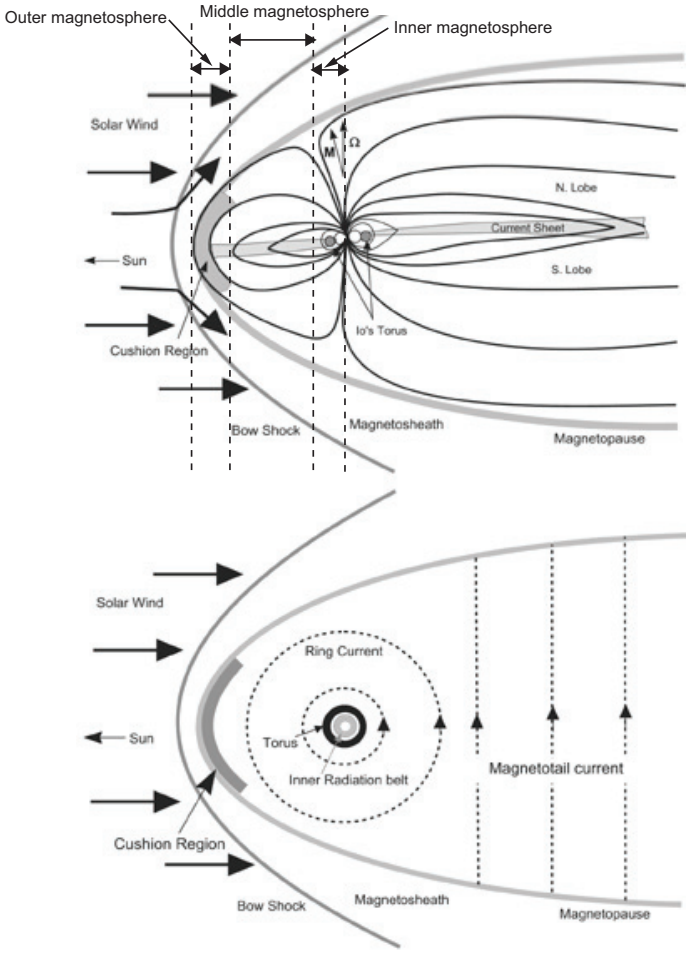

Figure 1.1: A schematic of Jovian magnetosphere showing the noon-midnight meridian (top) and the equatorial cross section (bottom) [*Khurana et al.*, 2004].

nightside, they are stretched down tail until they pinch off and launch plasmoids down the tail (Figure 1.2). *Cowley et al.* [2003] and *Stallard et al.* [2003] combined this Jupiter driven system with an IMF reconnection driven system (the Dungey cycle) to form a description of the overall convection in the Jovian magnetosphere (Figure 1.3). They obtained support for this model from using Doppler measurements of infrared Jovian auroras. *Southwood and Kivelson* [2001] and *Cowley and Bunce* [2001] have argued that the effects of changes in the solar wind dynamic pressure can extend into the middle magnetosphere and influence the rotating current sheet. For instance, increasing the dynamic pressure compresses the magnetosphere, and the conservation of angular momentum causes the plasma to rotate more rapidly.

So far seven spacecrafts (Voyager 1/2, Pioneer 10/11, Ulysses, Galileo and Cassini) have probed the Jovian magnetosphere as shown in Figure 1.4. Thanks to the database

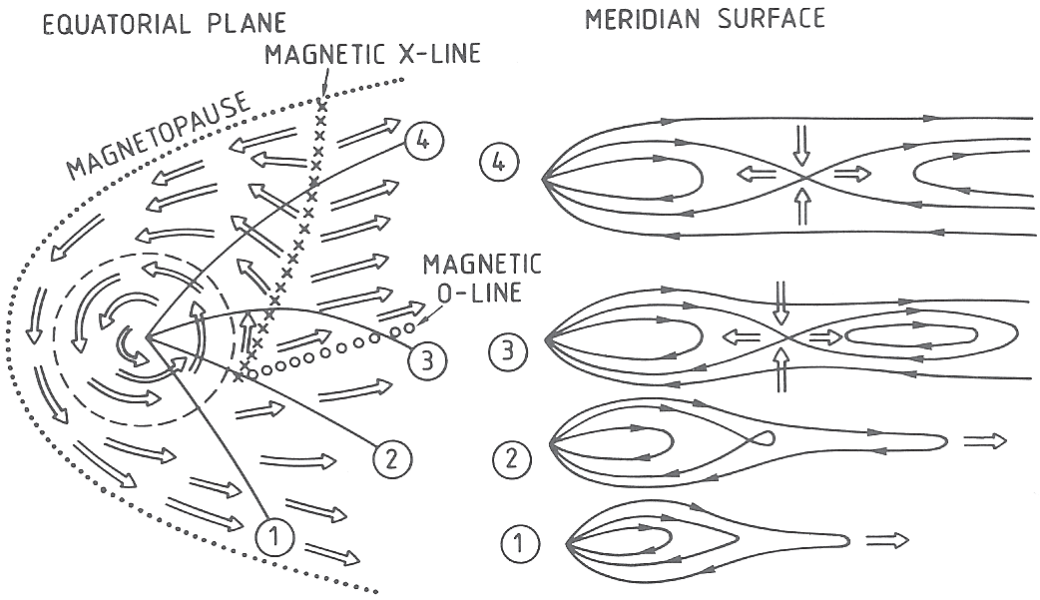

Figure 1.2: Qualitative sketch of plasma flow in the equatorial plane (left) and of the associated magnetic field and plasma in a sequence of meridian surfaces (right) expected from the planetary wind model [*Vasyliunas*, 1983]. This sequence is so called the Vasyliunas cycle.

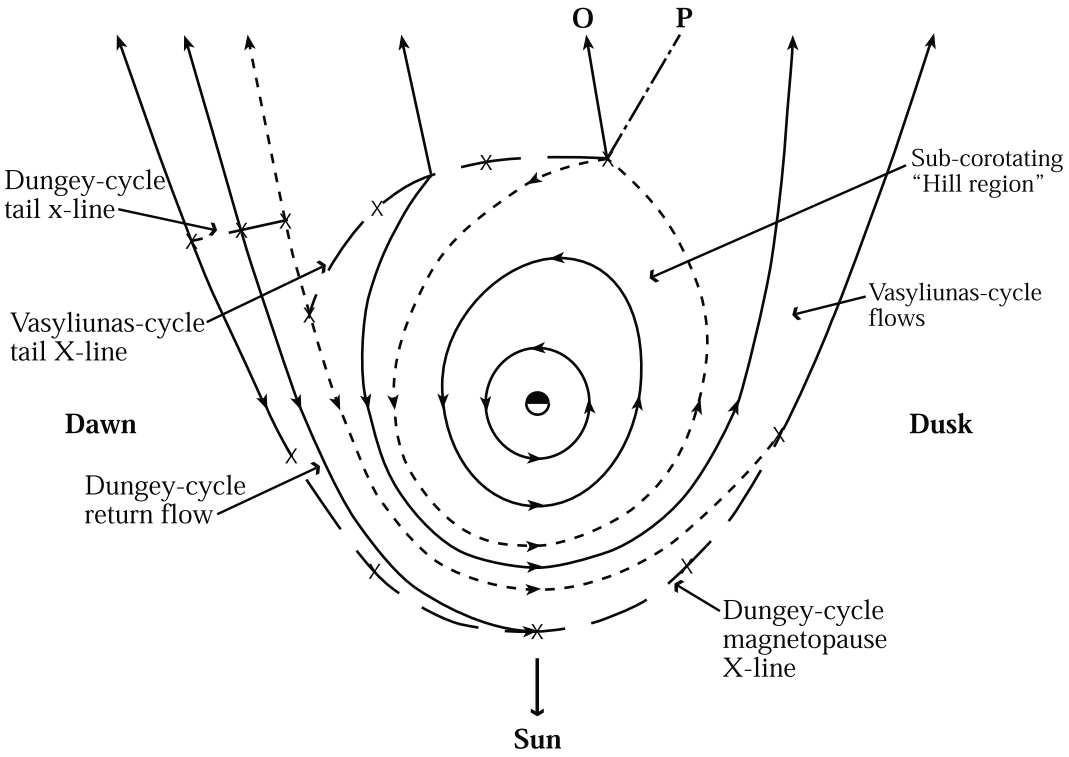

Figure 1.3: Sketch of the flows in the jovian equatorial plane [*Cowley et al.*, 2003].

from these missions we now have a good picture of the overall configuration of Jovian magnetosphere [e.g. *Joy et al.,* 2002]. *Joy et al.* [2002] described the shape of the bow shock and magnetopause by fitting the simulation results with polynomials. In addition they summarized the huge volume of observational data and established probabilistic models of the bow shock and magnetopause. A number of simulation studies [*Ogino et al.*, 1998; *Miyoshi and Kusano*, 1997; 2001; *Walker et al.,* 2001; 2005; *Walker and Ogino,* 2003] have considered the overall magnetospheric configuration for a range of solar wind dynamic pressures and IMF orientations. Simulations without an IMF show the basic *Vasyliunas* [1983] picture with inertial reconnection in the early morning plasma sheet [*Ogino et al.*, 1998]. In the simulations the middle magnetosphere is dominated by the equatorial current sheet but the magnetic field becomes more dipolar near the magnetopause indicating the presence of a cushion like region [*Ogino et al.*,

1998; *Walker et al.*, 2001]. With a northward IMF solar wind driven reconnection as well as inertial reconnection occurs in the model plasma sheet provided that the IMF is northward long enough [*Walker et al.*, 2001; *Walker and Ogino*, 2003]. In all of these simulation studies the simulations were run until a quasi-steady magnetosphere resulted.

The Galileo Energetic Particles Detector (EPD) observed the flow bursts which reoccurred every 2 to 3 days [*Woch et al.*, 2002]. These bursts included Jupiterward and tailward flows. Plasma flow in this region is most always dominated by rotation [*Krupp et al.*, 2001]. *Woch et al.* [2002] suggested that the flow bursts observed in the outer Jovian magnetosphere are related to plasma injections observed in the inner magnetosphere. In addition, studies of auroral radio emissions, *Louarn et al.* [1998, 2000] have reported changes in the flux of auroral radio emissions and radiation from the Io torus that may correspond to magnetodisc fluctuations with periods of 50 to 80 hours. Additionally, *Reiner et al.* [2000] argue that the long-term behavior of Jovian broadband kilometric (bKOM) and narrowband kilometric (nKOM) radio emissions observed during the Ulysses-Jupiter encounter were controlled by the sector structure of the solar wind.

1.2 Configuration and Dynamics of Kronian Magnetosphere

The configuration and dynamics of the Earth's magnetosphere are largely controlled by the solar wind while Jovian magnetosphere is dominated by its massive rotating equatorial current sheet and plasma source at Io. On the Earth magnetospheric activity is primarily driven by the interplanetary magnetic field (IMF). For southward IMF dayside reconnection between the Earth's magnetic field and the IMF drives the

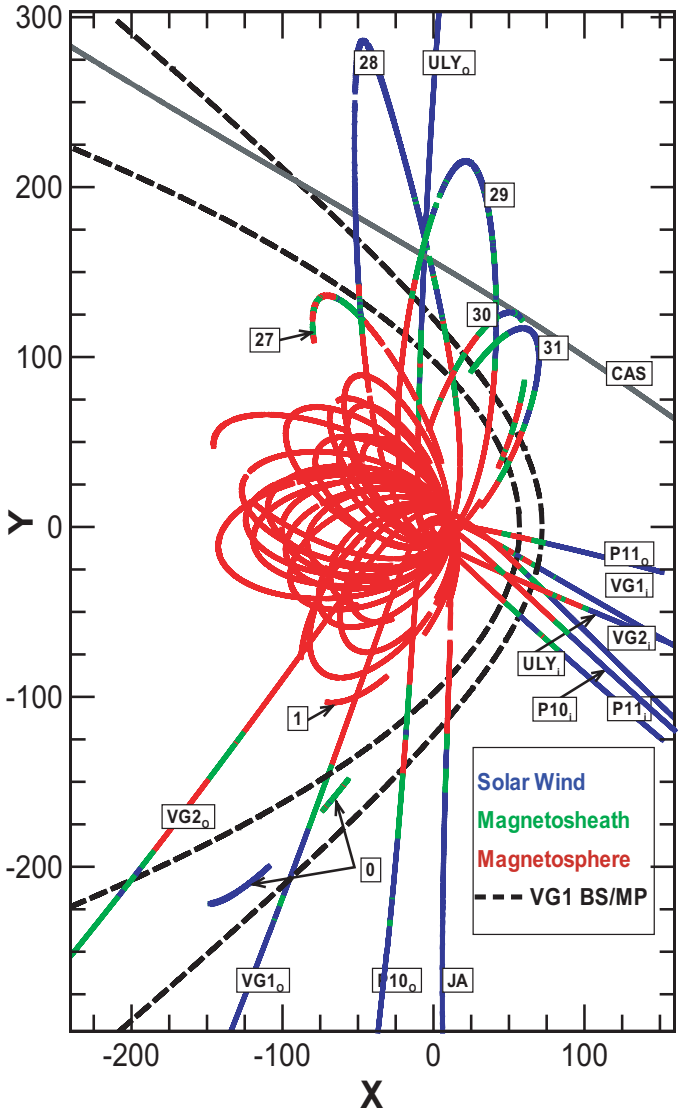

Figure 1.4: Summary of Jupiter observations to date. Trajectory data are colored red to indicate when the spacecraft was in the outer magnetosphere, green when in the magnetosheath, and blue when in the solar wind, and are dotted when the data are not used in this study (Cassini, Galileo after Feb 1, 2001). Individual spacecraft trajectories are labeled by using subscripts on the inbound (i) and outbound (o) portions of the trajectories. Galileo orbits crossing boundary surfaces are labeled by using orbit number (JA = Jupiter Approach, 0 = orbit 0, etc.). Except for Ulysses and Pioneer 11 outbound passes, all trajectories are near the Jupiter equatorial plane.

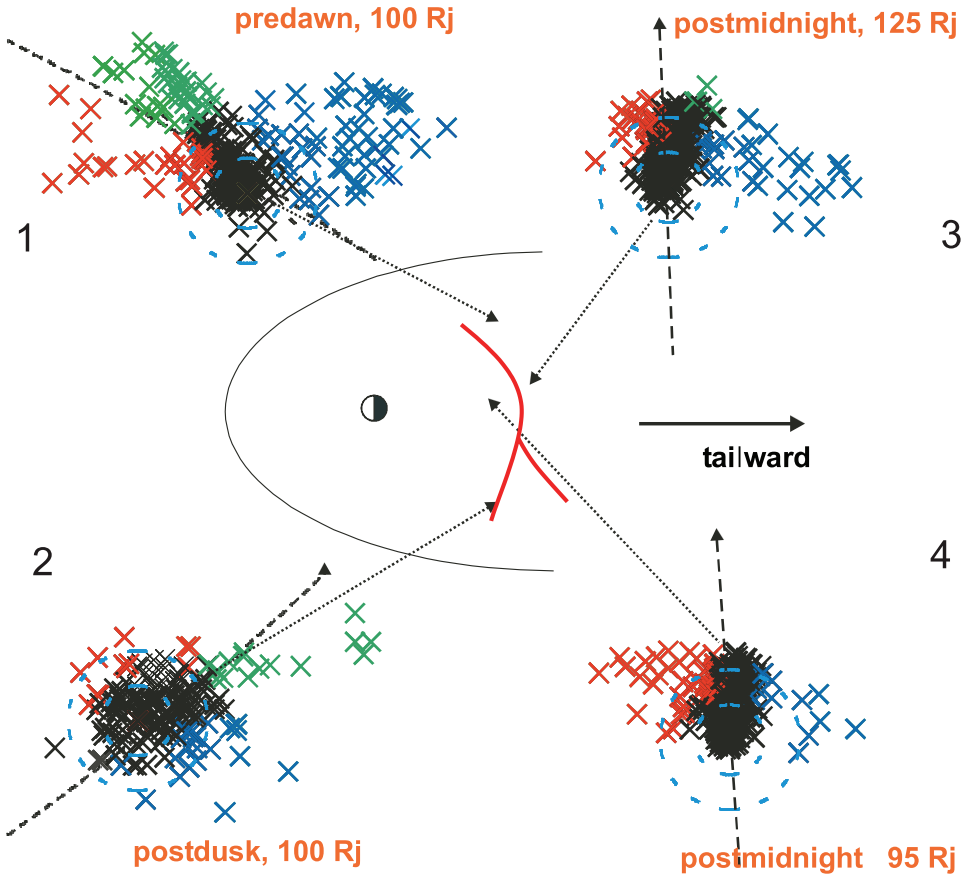

Figure 1.5: Deviations from the average pattern - particle flow burst distribution [*Woch et al.*, 2002]. Each anisotropy vector is plotted as a colorcoded dot, with: black - anisotropies not deviating significantly from the average anisotropy in the respective bin, green - anisotropies of enhanced magnitude but without directional deviation, blue - burst events defined by an enhanced magnitude and a directional deviation into the outward direction (away from Jupiter) red - bursts with an inward deviation (towards Jupiter). At the right: Bins from the same local time sector, but at different radial distances of 95 R_J (4) and 125 R_J (3), showing the transition from radial inward to radial outward flow bursts. At the right: bins from the same radial distance (100 R_J) but different local times sectors at dawn (1) and dusk (2), showing the predominance of bursts in the dawn sector. Dashed lines indicate the corotation.

magnetic flux transport to generate magnetospheric substorms and aurorae, while for northward IMF reconnection on the high latitude magnetopause of the polar cusp leads to a quiescent magnetosphere. On Jupiter aurorae and dynamics are primarily related to the currents that enforce rotation of the equatorial plasma. The solar wind has some influence at Jupiter (e.g. it has a long tail) and the details of the solar wind effects are still the subject of active research.

Saturn was thought to have aspects similar to both Jupiter and the Earth with internally driven and solar wind driven dynamics. Here we show the schematic of Kronian magnetosphere with considering the Cassini observational results as Figure 1.6. The polarity of the magnetic field is reversal of Earth's one. Recently *Crary et al.* [2005] have examined the relationship between solar wind parameters and the Kronian aurorae by using observations from the Cassini spacecraft as it approached Saturn and auroral images from the Hubble Space Telescope (HST) in January 2004 (Figure 1.7). During an interval with two corotating interaction regions (CIRs) they found that unlike Jupiter, Saturn's aurorae respond strongly to solar wind conditions. They further found that unlike the Earth, the solar wind dynamic pressure and total electric field primarily control the interaction rather than the north-south component of the IMF. Although *Bunce et al.* [2006] have suggested that dayside auroral emissions in the "cusp" are controlled by reconnection. *Cowley et al.* [2005] suggested that compression induced reconnection could account for both the correlation of auroral activity with CIRs and changes in the size of the auroral oval. Their model thus coupled the effects of enhanced pressure with reconnection. *Badman et al.* [2005] used the size of the polar cap to estimate the flux in the tail and the reconnection rate.

Hansen et al. [2005] used a global magnetohydrodynamic (MHD) simulation of the solar wind interaction with Saturn based on Cassini upwind observations just prior to encounter. They included a plasma source from Enceladus and got reasonable agree-

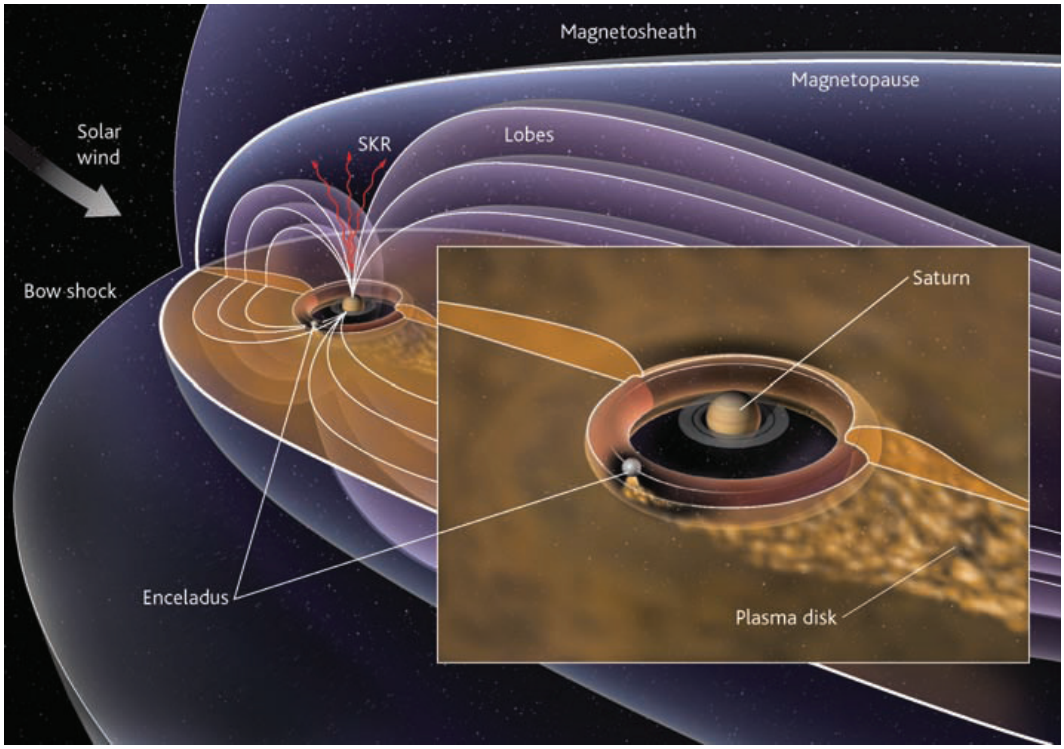

Figure 1.6: Schematic of Kronian magnetosphere showing the plume at Enceladus as the source of plasma and outflowing plasma on the night side in a region linked magnetically to a region of lower-than-average ionospheric conductance [*Kivelson*, 2006]. Red arrows indicate kilometric radiation emitted from Saturn's polar region (SKR). Diagram is not to scale.

ment between the simulation and observed boundaries.

1.3 Description of the Dissertation

As described above, rapidly rotating giant planet Jupiter and Saturn have a characteristic configuration and dynamics of the magnetosphere. In this thesis we clarify Jovian and Kronian magnetospheric configuration with three dimensional global MHD simulation. In particular we establish the Jovian magnetospheric configuration under the lower solar wind dynamic pressure and reveal why the periodic plasma flow occur in the tail. At Saturn we bring out whether the directions of IMF affect the aurora

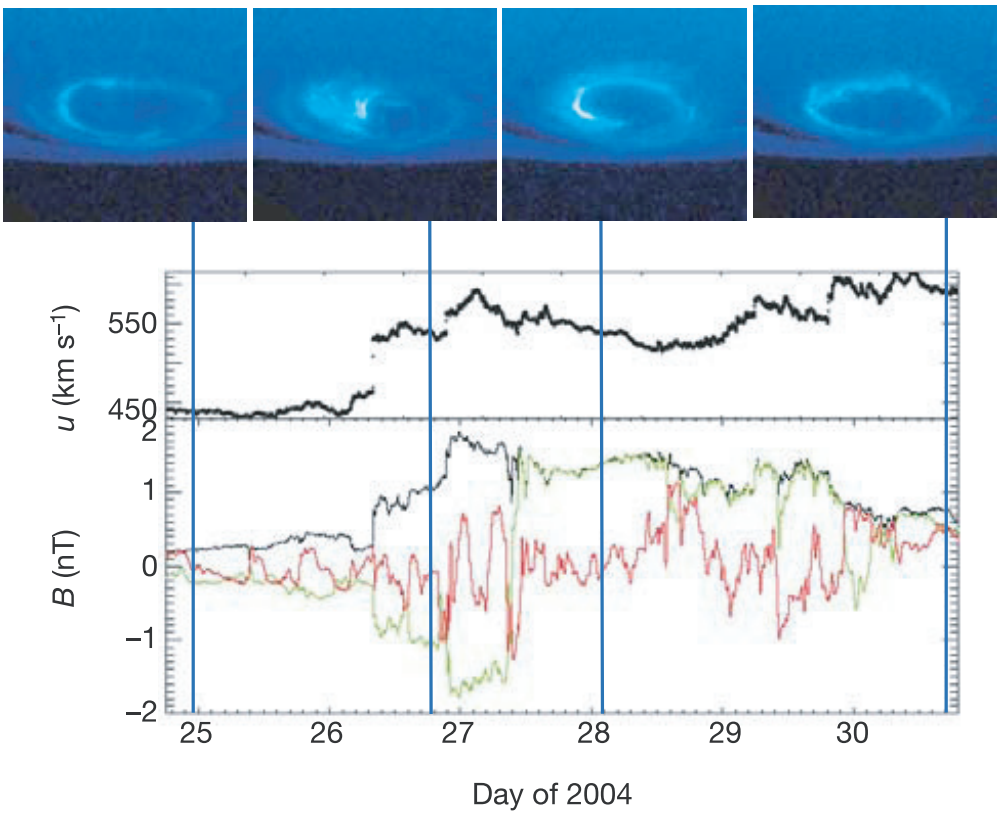

Figure 1.7: Comparison between HST images and solar wind conditions propagated to Saturn for the period 25-30 January 2004 [*Crary et al.*, 2005]. Thick blue vertical lines indicate the times of the four HST images shown above. The solar wind conditions are measured by Cassini. The top panel shows the flow speed, and the lower panel the magnetic field. The black line shows the magnitude of the magnetic field. B_Y is in green and B_Z is in red. The magnetic field is in planetary coordinates, a right-handed system with z parallel to the axis of rotation (and magnetic moment), and the Sun in the +x/z half-plane.The density and the B_X component are omitted for clarity. In one-dimensional, time-dependent magnetohydrodynamics with a uniform upstream boundary condition, the x component cannot be accurately modelled. The modelled propagation times may be systematically long by as much as 10 h. Non-radial orientation of the solar wind structures, typical of corotating interaction regions, could cause them to reach Saturn roughly five hours earlier than spherically symmetric calculations would suggest. Solar rotation and the 3.38 difference between the spacecraft's and Saturn's heliocentric longitude could also move arrival times earlier by approximately 6 h. Overall, the estimated arrival times may be systematically late by up to roughly 10 h.

brightness.

In this dissertation first we describe characters and recent studies of Jupiter and Saturn and mention the purpose of this thesis in Chapter 1. Then the basic equations and simulation model are shown in Chapter 2. In Chapter 3 we obtain the simulation results of the periodic reconnection. We were also interested in finding out whether this phenomenon could account for the periodicity observed in the EPD flow bursts and the auroral emissions. In this study we use the dependent three dimensional MHD simulation of the interaction between the Jovian magnetosphere and the solar wind that was used in the earlier studies [*Ogino et al.,* 1998]. Also we examine the configuration of the magnetosphere during a series of simulations both with and without an IMF to determine parameters that control the location of the rotating current sheet, cushion region and magnetopause. Then we vary the solar wind parameters to determine the relationship between periodic reconnection and steady reconnection. Finally we discuss these results and present a model of the response of the Jovian magnetosphere to a northward IMF turning. Then in Chapter 4 we present the results of a study of the interaction of the solar wind with Saturn by using a three dimensional global MHD simulation in which we include a source of plasma in the inner magnetosphere. In particular we examine the effects of solar wind changes on the size of the magnetosphere, the convection within the magnetosphere and the field-aligned currents and energy flux to the Kronian ionosphere. We compare and contrast our Kronian results with those at Jupiter and the Earth. Finally conclusions are summarized in Chapter 5.

Chapter 2

Simulation Model

2.1 MHD Equations

In this chapter the MHD simulation model which is applied to the simulation of both Jovian and Kronian magnetosphere is described.

Most of the space is filled with the charged particle and electro-magnetic field. There are two ways to deal with the interaction between the particle and the field. One way is that plasma is treated as particles to calculate the each particle trajectory with Newton kinetic equation. This gives apercus of the behavior of ionized gas, however it needs to consider the interaction among the effect of each particle. This is caused by that the kinetics of particle combination makes charge and current, which vary the original electro-magnetic field. The other is the way plasma is treated as fluid to use MHD equations. This way does not need to consider the both particle-particle and particle-field interactions, therefore this is unable to describe the effect of plasma kinetic effects.

It is general that plasma in space is collisionless because the mean free path of particle is enough large with the extremely low density. We usually use the ratio between

frequency of the phenomena ω and the frequency of collision ν when we evaluate the importance of collision. when $\nu << \omega$ is satisfied, plasma is collisionless. Although the hydrodynamic equations are originally derived when $\nu >> \omega$, it is thought that the equations can approximate plasma when the distribution function of velocity is close to the Maxwell distribution even if $\nu << \omega$; here ν should be lower than the ion gyro frequency, the equations are applied to the broad frequency domain. MHD equations consist of both the equation of magnetic filed variation and the hydrodynamic equation. MHD equations are derived from the Vlasov (Collisionless-Boltzmann) equation and describes one fluid model with the combination of the equation of electrons and ions. The equation is applicable to the phenomena which the particle effect of plasma is not so significant, namely the phenomena is long wavelength and slower than the cycle of ion gyro-frequency. In this study we employ the MHD equation to investigate the configuration and dynamics of the global Jovian magnetosphere. The normalized MHD equations and Maxwell equations which are based on the MHD model are

$$\frac{\partial \rho}{\partial t} = -\nabla \cdot (\mathbf{v}\rho) + D\nabla^2\rho \tag{2.1}$$

$$\frac{\partial \mathbf{v}}{\partial t} = -(\mathbf{v} \cdot \nabla)\mathbf{v} - \frac{1}{\rho}\nabla p + \frac{1}{\rho}\mathbf{J} \times \mathbf{B} + g + \frac{\mathbf{\Phi}}{\rho} \tag{2.2}$$

$$\frac{\partial p}{\partial t} = -(\mathbf{v} \cdot \nabla)p - \gamma p \nabla \cdot \mathbf{v} + D_p\nabla^2 p \tag{2.3}$$

$$\frac{\partial \mathbf{B}}{\partial t} = \nabla \times (\mathbf{v} \times \mathbf{B}) + \eta\nabla^2\mathbf{B} \tag{2.4}$$

$$\mathbf{J} = \nabla \times (\mathbf{B} - \mathbf{B}_d) \tag{2.5}$$

where ρ is the plasma density, $\mathbf{v}$ the plasma velocity, p the plasma pressure, $\mathbf{B}$ the magnetic field and $\mathbf{J}$ the current density. $\mathbf{B}_d$ is the dipole magnetic field of the planet, g the force of gravity, $\mathbf{\Phi} \equiv \mu\nabla^2\mathbf{v}$ the viscosity and $\gamma = 5/3$ is the ratio of specific heat. The resistivity, $\eta = \eta_0(T/T_0)^{-3/2}$, has the classical temperature dependency, where $T =$

p/ρ is the temperature and T_0 is the ionospheric temperature. The model resistivity η_0 is set to 0.001 and the diffusion coefficients are $D = D_p = 0.001$. The magnetic Reynolds number is $S = \tau_\eta/\tau_A$ = 100-2000, where $\tau_\eta \equiv \Delta x^2/\eta$ and $\tau_A \equiv \Delta x/v_A$. Δx is the mesh size and v_A is the Alfvén velocity. The numerical Reynolds number is 5 times larger than the magnetic Reynolds number.

The diffusion and viscous terms are added to suppress MHD fluctuations which come from unbalanced forces of the difference approximation at the start of the calculation. These numerical oscillations tend to occur at the bow shock and magnetopause and have a scale length that is the same as the grid spacing. This does not affect the magnetospheric configuration very much because the numerical forces between neighboring meshes tend to cancel out each other. The very small viscous and diffusion coefficients used in the calculations are sufficient to suppress these oscillations. This is eapecially important in the relatively narrow region between the magnetopause and bow shock, where the oscillations can interfere with each other.

Chapter 3

Jovian Magnetospheric Dynamics

3.1 Jovian Simulation Model

Our simulation model of the solar wind interaction with Jupiter's rapidly rotating magnetosphere has been described by *Ogino et al.* [1998]. In this section we briefly review the simulation model and show how this calculation differs from previous calculations.

The simulation was approached in two stages. First, we develop a model for a steady state spinning magnetized plasma, and then we use that model as the initial state for a global MHD simulation of the interaction of the solar wind with a rotating magnetosphere.

To model the plasma and field configuration near Jupiter, at the initial time $t = 0$, an image dipole is placed upstream of Jupiter to hasten the formation of the magnetopause and help to assure $\nabla \cdot \mathbf{B} = 0$ throughout the simulation box [*Watanabe and Sato*, 1990]. An unmagnetized solar wind is launched with a dynamic pressure of $\rho v_{sw}^2 = 0.75$ nPa ($v_{sw} = 300$ km s^{-1}) and a temperature of 2×10^5 K from the upstream boundary of the simulation box. We solve the resistive MHD equations as an initial value problem by using the Modified Leap-Frog Method described by *Ogino et al.* [1992]. The

approach used in calculating the difference equations satisfies $\nabla \cdot \mathbf{B} = 0$, however on the boundary condition this calculation does not guarantee $\nabla \cdot \mathbf{B} = 0$; therefore we monitor the error in $\nabla \cdot \mathbf{B} = 0$ which is given by $E = |\Delta x(\nabla \cdot \mathbf{B})/B|$ where Δx is the grid spacing. E is typically $\sim 10^{-4}$ and becomes less than $\sim 10^{-3}$. Our MHD model is one fluid model so that we cannot treat the effects of multi-species problems. The Jovian magnetosphere was modeled on either a $602 \times 402 \times 202$ or a $452 \times 302 \times 152$ point Cartesian grid with a grid resolution of 1.5 R_J (R_J is 1 Jovian Radius). This resolution is suited to the major part of Jovian magnetosphere, however this cannot describe the small magnetospheric configuration such as the thin (~1 R_J) plasma sheet.

The magnetic field is fixed to the values of the Jupiter's internal dipole and does not include the 10^o magnetic dipole tilt. The magnetic polarity of Jupiter is opposite to Earth's magnetic field. In the simulation, 1×10^{30} - 7×10^{30} ions s^{-1} pass through a surface at 22.5 R_J into the Jovian system. We use the actual values for each run in Table 3.4. These values are within the expected range [*Hill et al.,* 1983]. In addition we ran one case for which the densities within 15 R_J were five times the Voyager 1 values. This makes it possible to investigate the influence of the inner boundary condition on the results and to test our ideas about the effects of reconnection. In this study we set the IMF magnitude to 0 nT, ±0.105 nT and ±0.420 nT and set the dynamic pressure to 0.011 nPa, 0.023 nPa, 0.045 nPa and 0.090 nPa. These values are at the lower end of the range observed in the solar wind near Jupiter's orbit (mean ρv^2 = 0.09 nPa; mean B = 0.8 nT) [*Smith et al.*, 1978; *Bridge et al.*, 1979a, b; *Philips et al.*, 1993; *Joy et al.* 2002]. The dynamic pressures vary with changing solar wind density.

3.1.1 Initial Conditions

The initial pressure, density, and temperature of the plasmas from the ionosphere and inner magnetosphere were determined by assuming a hydrostatic equilibrium in the

absence of a magnetic field and rotation:

$$\frac{1}{\rho}\frac{dp}{dr} + \frac{g_0}{r^2} = 0 \tag{3.1}$$

where g_0 is the coefficient of gravity, p is the pressure, ρ is the mass density, and r is the radial distance from Jupiter in Jovian radius. If we assume $T = T_0 r^l$ and $m = m_0 r^{-k}$ where l and k are positive, then hydrostatic solution such as $\rho = \rho_0 \exp\theta/r^{l+k}$ and $p = p_0 \exp\theta$ are obtained by using $p = \rho T/m = p_0 \rho r^{l+k}/\rho_0$ where m is the effective mass per ion, T is the temperature, $\theta \equiv \sigma((1/r^{l+k+1}) - 1)$ and $\sigma \equiv \rho_0 g_0/(p_0(l + k + 1))$. The density is normalized by $n_0 = 1$ so that $\rho_0 = m_0 n_0 = m_0$. The functional forms for $T(r)$ and $m(r)$, and therefore $\rho(r)$ and $p(r)$ are chosen so the model temperature and mass density have a radial dependence like that observed in the inner magnetosphere on Voyager 1. The model parameters were adjusted to fit the Voyager 1 observations and by assuming pressure balance between the Jovian plasma and the solar wind ram pressure (0.75 nPa) at $r_{mp} = 52.5$ R_J beyond which ρ and p were set to solar wind values. The parameters used for the initial Jovian plasma are given in Table 3.1.

Table 3.1: Parameters for Internal Plasma

Parameter	Value
l	0.378
k	0.493
m_0	7.04
σ	9.41

The initial condition on the velocity were determined by developing a steady state model of a rapidly rotating magnetospheric configuration. This calculation was carried out in two dimensions since in the absence of the solar wind the configuration has azimuthal symmetry. It was found that starting with these initial steady state models reduces start-up fluctuations and helps us to attain a quasi-steady configuration for the magnetosphere more rapidly since the simulation began.

In cylindrical coordinates (R, φ, z) with $v = v_\varphi \hat{\varphi}$ ($\hat{\varphi}$ is the unit vector) the momentum equation becomes

$$-\rho\omega^2 R + \frac{\partial p}{\partial R} - J_\varphi B_z + J_z B_\varphi = 0 \tag{3.2}$$

$$-\frac{1}{\rho}(J_z B_R - J_R B_z) = 0 \tag{3.3}$$

$$\frac{\partial p}{\partial z} - J_R B_\varphi + J_\varphi B_R = 0 \tag{3.4}$$

where ω is the rotation frequency of Jupiter, $\mathbf{J}$ is the current density and $\mathbf{B}$ is the magnetic field. We assume that the magnetic field can be expressed as

$$\mathbf{B} = \frac{\mathbf{1}}{\mathbf{R}}\nabla\psi \times \hat{\varphi} + \mathbf{B}_\varphi \hat{\varphi} \tag{3.5}$$

where ψ is the magnetic flux. In (3.2) B_R and B_Z are dipolar. Since we have assumed time independence, the induction equation ($\partial B/\partial t = \nabla \times (\mathbf{v} \times \mathbf{B}) = 0$) and φ component of the momentum equation are satisfied if $v_\varphi/R = \omega(\psi)$ and $RB_\varphi = I(\psi)$. Since ω must be a function of ψ due to time independence, we selected velocities of the form

$$v_\varphi = \frac{\omega_0 R \psi^M}{\psi^M + \psi_0^M} \tag{3.6}$$

where M is integer, $\omega_0 = 1.76 \times 10^{-4}$ is the corotation frequency, ψ_0 is the value of ψ at $R_0 \approx 35$ R_J comes from $\rho v_\varphi^2 = B_z^2$ for the initial configuration. At the equator, ψ can be found from $\psi = R_0/R\psi_0$. In this model we present the results from the simulation for which $M = 2$ model was used as the initial state for our MHD simulations This gives

$$M = 2: \quad v_\varphi = \frac{R\omega_0}{1 + (R/R_0)^2} = \begin{cases} \omega_0 R_0^2/R, & \text{for } R >> R_0 \\ \omega_0 R, & \text{for } R << R_0 \end{cases} \tag{3.7}$$

Equation (3.7) approximates *Hill*'s [1979] solution based on uniform radial outflow in a dipole field with large R (see Figure 2 of *Hill* [1979]).

3.1.2 Boundary Conditions

In the simulation the magnetic field (**B**), velocity (**v**), mass density (ρ) and thermal pressure (p) are maintained at solar wind values at the upstream boundary (x = 300 or 225 R_J) while free boundary conditions, through which waves and plasmas can freely leave the system, are used at the downstream ($x = -600$ or -450 R_J), side ($y = \pm 300$ or ± 225 R_J), and top (z = 300 or 225 R_J) boundaries. Symmetry boundary conditions are used at the equator ($z = 0$). At the inner magnetosphere boundary all of the simulation parameters (**B**, **v**, ρ, p) are fixed for r <15 R_J. This boundary is the main source of plasma for the simulation [*Walker and Ogino*, 2003]. Therefore our simulation model cannot treat the inner (< 15R_J) magnetospheric dynamics including Io torus. The density gradient established by the boundary condition allows mass to be transported out to the magnetosphere. The simulation quantities are connected with the inner boundary through a smooth transition region ($15 < r < 21$ R_J). Also we connect the current to the ionosphere through this transition region as that current becomes zero on the surface of the ionosphere. For $r < 21$ R_J each parameter φ was calculated by using

$$\varphi(r,t) = f\varphi_{ex}(r,t) + (1-f)\varphi_{in}(r) \tag{3.8}$$

where $\varphi_{ex}(r,t)$ is the value from the simulation and $\varphi_{in}(r)$ is the value from the initial model. The value of f depends only on the radial position and is given by

$$f \equiv \frac{a_0 h^2}{a_0 h^2 + 1} \tag{3.9}$$

where a_0= 30 R_J and

$$h \equiv \frac{r^2}{r_a^2} - 1, \quad r \geq r_a \tag{3.10}$$

$$h \equiv 0, \quad r < r_a \tag{3.11}$$

with r_a= 15 R_J.

The numerical stability criterion is $v_g^{\max}\Delta t/\Delta x < 1$ where $v_g^{\max}$ is the maximum group velocity in the calculation domain and Δt is the time step. Since the Alfvén velocity becomes very large near Jupiter due to the huge magnetic field, the inner boundary of the simulation was placed at 15 R_J in order to avoid the too small time step. Within 15 R_J the velocity is purely rotational and the pressure and density are set to values determined from the Voyager 1 flyby of Jupiter [*Belcher*, 1983].

3.2 Configuration of Jovian Magnetosphere

In this section we describe the overall magnetospheric configuration that results from our Jovian simulations and in the next section we put the dynamics into the context of the global configuration. First we modeled the magnetosphere without an IMF. We started by adjusting the solar wind mass density to give a solar wind dynamic pressure of 0.090 nPa. After 100 hours we decreased the dynamic pressure by half to 0.045 nPa and ran the simulation for an additional 37 hours. At t = 137 hours we further reduced the dynamic pressure to 0.023 nPa and finally the dynamic pressure was set to 0.011 nPa at t = 178 hours. After that the pressure was held constant for 50 hours then either a northward or southward IMF of 0.105 nT was imposed to obtain two additional results.

In each case the magnetosphere reached a quasi-steady state when we changed the pressure. For the cases without an IMF, the quasi-steady state in the Jovian magnetosphere results from a pressure balance between the solar wind dynamic pressure, the magnetic pressure and tension of Jupiter's magnetic field, the thermal pressure of its plasma and the centrifugal force caused by the Jovian rotation. Table 3.2 shows the distance to the magnetopause and bow shock from Jupiter at each pressure change. The magnetopause and bow shock were defined from the sharp pressure gradients at the

boundaries. Figure 3.1 shows the distributions of magnetic field (top panel), plasma velocities (middle panel), thermal pressure and mass density along the Sun-Jupiter line with the solar wind dynamic pressure of 0.011 nPa and no IMF. Examples of the pressure gradients are indicated by circles 3 and 4 in Figure 3.1. At the low pressures used in these simulations the magnetosphere has an irregular cross section (Table 1 and Figure 1 of *Walker et al.* [2005]). It is closer to Jupiter at dawn than at dusk. At dawn the corotational flow is opposite to the solar wind, on the other hand at dusk both the corotational flow and the solar wind stream into the night side. Finally the magnetosphere is flattened. The northern and southern magnetopauses are closer to Jupiter than at the flanks. The space between the magnetopause and bow shock (magnetosheath) increases as the dynamic pressure decreases (see *Ogino et al.* [1998], *Joy et al.* [2002] and *Walker et al.* [2005]). Table 3.3 shows the corotation boundary distance at dayside and nightside, and the thickness of "cushion region" and neutral line in the tail with each pressure. For lower solar wind dynamic pressure the magnetopause is easy to inflate and the thickness of the "cushion region" increases. We defined thickness of the "cushion region" as the equatorial distance between the magnetopause and the position where the steep gradient in corotation velocity vanishes. Circles have been drawn around the velocity slope changes in the middle panel of Figure 3.1 and these have been labeled 1 and 2. Thus in Table 3.3 the cushion is the region between 1 and 4. In Figure 3.2 the cushion region at noon lies between the red lines labeled 1 and 4.

The size of the cushion region depends on the solar wind dynamic pressure. For a dynamic pressure of 0.090 nPa the cushion is 8 R_J thick. This is about 10% of the standoff distance of the magnetopause. For ρv_{sw}^2 = 0.045 nPa and 0.023 nPa the ratios are 17% and 20%, respectively, while for ρv_{sw}^2 = 0.011 nPa it is 30%. For a high solar wind dynamic pressure, this finding suggests that processes at the magnetopause such as reconnection may directly influence the current disk while for lower pressures the

Table 3.2: The dependence of the magnetopause and bow shock locations on the solar wind dynamic pressure (P_{Dyn}) and IMF B_Z. X, Y and Z indicate the directions in the same as Figure 3.2. Y_{avg} is the average distance at dawn side (Y_{dawn}) and dusk side (Y_{dusk}). X_b and X_m are the position of bow shock and magnetopause, respectively.

		Magnetopause (R_J)					Bow Shock (R_J)					BS to MP Standoff Ratio
P_{Dyn}(nPa)	B_Z(nT)	X	Y_{avg}	Z	Z/Y_{avg}	Y_{dawn} /Y_{dusk}	X	Y_{avg}	Z	Z/Y_{avg}	Y_{dawn} /Y_{dusk}	X_b/X_m
0.090	0	76	112	107	0.95	0.94	100	174	173	0.99	1.01	1.316
0.045	0	90	136	125	0.92	0.99	118	207	204	0.99	1.03	1.311
0.023	0	102	152	133	0.88	0.96	126	221	225	0.96	1.00	1.235
0.011	0	119	170	137	0.81	0.98	155	261	250	0.96	1.00	1.30
0.011	0.105	117	159	149	0.94	0.95	144	231	250	1.08	0.96	1.22
0.011	–0.105	130	178	152	0.85	1.00	165	280	245	0.88	1.00	1.27

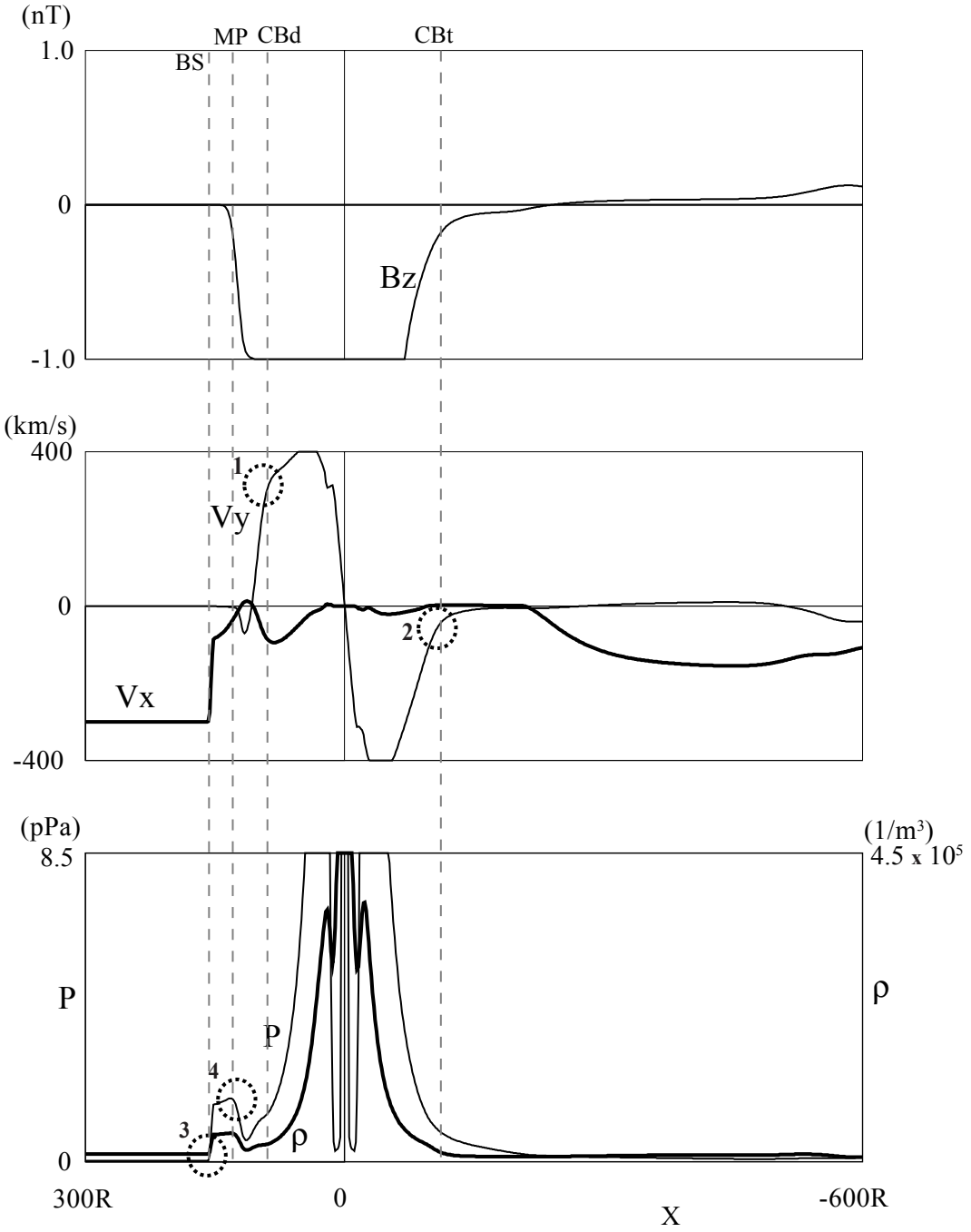

Figure 3.1: Magnetic field (top panel), plasma velocities (middle panel), thermal pressure and mass density along the Sun-Jupiter line. The solar wind dynamic pressure is 0.011 nPa and IMF is zero. Only the magnetic field z-component and the velocity x- and y-components are shown. The circles with numbers indicate the gradients which were used to determine several boundaries. The four dashed lines show the location of the bow shock (BS), the magnetopause (MP) and the corotation boundaries on the dayside (CBd) and in the tail (CBt).

Table 3.3: The subsolar distance to the corotation region, thickness of the cushion region and distance to the neutral line on the x-axis as a function of solar wind dynamic pressure (P_{Dyn}). The cushion region is between the magnetopause (X_m) and corotation boundary on the dayside ($X_{dayside}$). X_{tail} is also the corotation boundary in the tail. It was determined by using the velocity gradients circled in Figure 3.1. The neutral line ($X_{neutral}$) was defined as the location in the tail where the magnitude of B_Z becomes zero.

	Corotation boundary distance		Cushion region	Neutral line
P_{dyn}(nPa)	$X_{dayside}$ (R_J)	X_{tail} (R_J)	X_m-$X_{dayside}$(R_J)	$X_{neutral}$ (R_J)
0.090	68	90	8	-103
0.045	75	101	15	-133
0.023	81	115	21	-152
0.011	83	115	36	-219

influence on the middle magnetosphere will be less direct. In the cushion region the thermal pressure (< 2 pPa) and density remain relatively small while the magnetic field magnitude and rotation velocity (v_Y) increase. For northward IMF the magnetopause erodes due to dayside reconnection. The addition of reconnected magnetic flux to the tail lobes causes the polar magnetopause to move outward. In the case of Table 3.2 the average y-dimension stays larger than the z-dimension, but if the IMF is sufficiently large the magnetosphere becomes largest in the z-direction [*Walker et al.*, 2005]. For southward IMF the magnetosphere expanded in the x- and y-directions due to high-latitude reconnection which removed lobe flux.

The simulation results at t = 174 hours and t = 224 hours are shown in Figure 3.2 (a, b). Recall that the dynamic pressure is 0.023 nPa and 0.011 nPa at these times. In this figure the arrows show the plasma flow vectors while the color spectrogram gives the plasma temperature. The left panel is for the equatorial plane (z = 0) and the right panel is for the x = 0 plane. The black region near Jupiter is inside of the inner magnetosphere boundary (r < 15 R_J) and is not included in the calculation. The peak temperature is higher and the region of enhanced temperature is thicker and closer

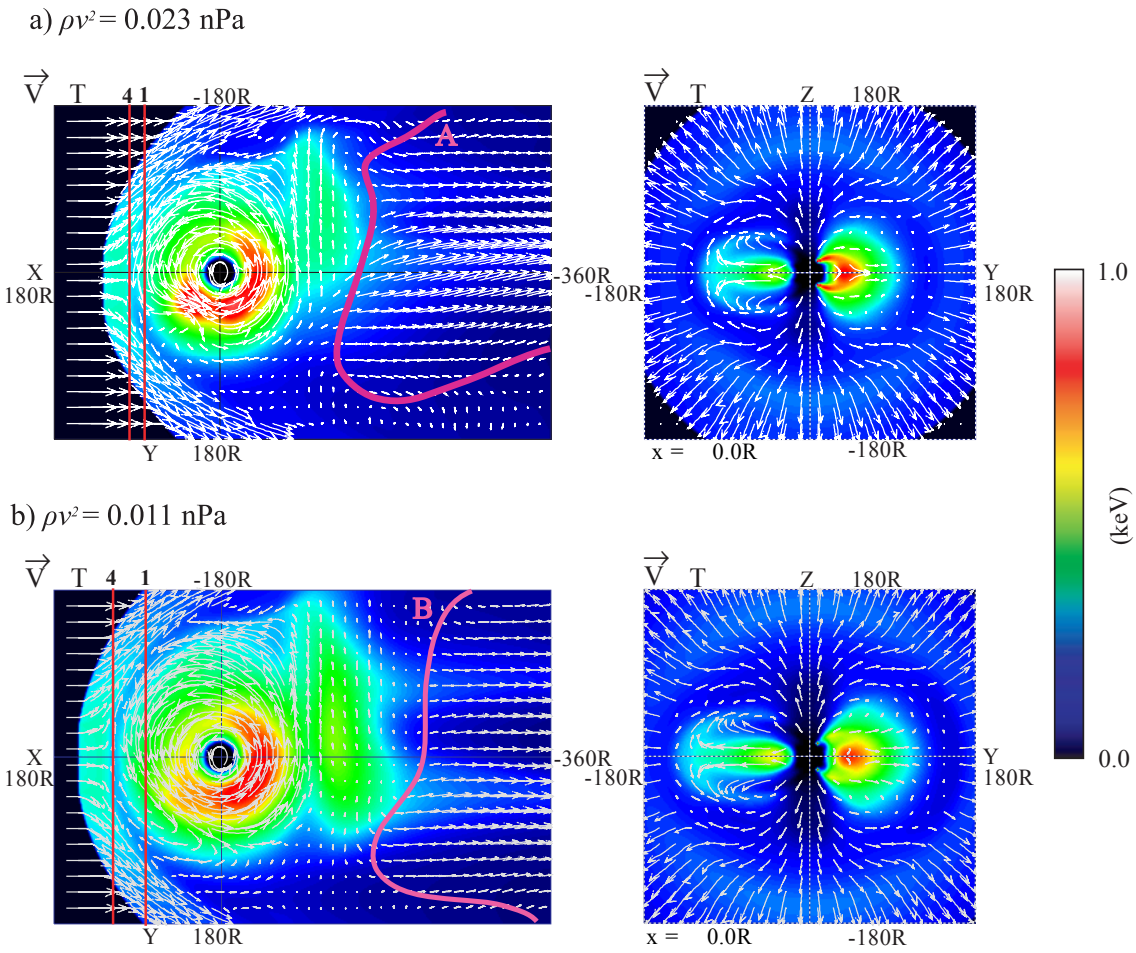

Figure 3.2: Temperature per atomic mass unit (AMU) and plasma flow vectors in the dawn-dusk meridian (yz) plane (right) and equatorial plane (left). The top panels contain simulation results with a solar wind dynamic pressure of 0.023 nPa and zero IMF at t = 174 hours while the bottom contains results with a dynamic pressure of 0.011 nPa and zero IMF at t = 224 hours. The color bar gives the temperature values. The magenta lines A and B show the neutral line. On the dayside two red lines show the magnetopause and corotation boundary at the sub-solar point from Table 3.3. The black region in the center of the panels is inside the inner boundary of the simulation at 15 R_J.

to Jupiter on the dusk side. In the left panel of Figure 3.2a, the temperature is high in a band extending from 1500 LT (local time) across the nightside to 0600 LT. The configuration of this region of enhanced temperature is controlled by the solar wind dynamic pressure (c.f. Figure 3.2a and b). The simulated Jovian magnetosphere has a strong dawn-dusk asymmetry. For instance, the plasma sheet is much thicker at dusk than at dawn [*Ogino et al.* 1998; Figure 2 right panels]. There is also a large dawn-dusk asymmetry in the flow. Across most of the night and morning the flow is characterized by both rotation and outflow. At dawn the region of rotation extends to about 120 R_J in Figure 3.2a. At about 1500 LT, however, the flow turns radially inward and the plasma is heated. At about dusk the flow again develops an outward component. The result is a region in the afternoon with very small flows. This behavior is regulated by the solar wind dynamic pressure. In the left panel of Figure 3.2b for lower dynamic pressure, the inward component of the flow in the afternoon is greatly reduced and the region of stagnation has been replaced by a vortex in which the flow actually reverses and moves opposite to corotation in the cushion region. At local noon the dawnward flow merges with solar wind induced flows to form a band of anti-corotation flows near the magnetopause.

The temperature in the afternoon region is smaller than in Figure 3.2a. These flow patterns are caused by the interaction of the solar wind and rotating Jovian plasma. In the morning the rotating Jovian flow is opposite to the solar wind flow while in the afternoon they are in the same direction. Furthermore flux tubes in the morning have an outward flow and a strong interaction with the magnetopause. They push the magnetopause away from Jupiter and become highly stretched in the process. When they rotate past noon into the afternoon, they no longer interact strongly with the boundary and snap back toward Jupiter. That is, due to the effect of not strong interaction, the tension of the magnetic field line works as a changing the field line from tail-like

to dipole-like. This interaction is greatly reduced when the dynamic pressure of solar wind decreases and the magnetopause moves away from Jupiter. The flow which moves opposite to corotation at dusk side generates around stagnation point where the magnetic tension works as mentioned above. There is no space for the flow to go sunward at high pressure in the cushion region, however there is the space enough to stream in sunward at lowest pressure. Also *Krupp et al.* [2001] compared the simulation results of *Ogino et al.* [1998] with the flow pattern from Galileo observational results. They indicates that the very small averaged flow derived from Galileo EPD measurements in the dusk sector may indicate that Galileo has indeed crossed a vortex regime which is the source of the sunward flow in our simulation results.

At around dusk the flow again begins to move outward. In the evening quadrant the outward moving, rotating flux tubes quickly become stretched and eventually reconnect. This is an inertial effect (recall $B_{IMF} = 0$) [*Ogino et al.,* 1998]. In the simulations with dynamic pressures > 0.023 nPa, the neutral line is on the dawn side, similar to that suggested by Vasyliunas (compare Figure 11.19 of *Vasyliunas* [1983] with Figure 3.2a). The exact pattern is controlled by the dynamic pressure. For instance, for 0.011 nPa the neutral line extends almost completely across the magnetotail (Figure 3.2b).

3.3 Dynamics of the Jovian Magnetosphere for Northward IMF

3.3.1 Periodic Plasmoid Ejection in Jupiter's Magnetotail

In this simulation we gradually reduced the solar wind dynamic pressure to $p = 0.01$ nPa while the IMF was constant ($B_z = -0.105$nT). The dynamic pressure used in this simulation is near the minimum observed by spacecraft near Jupiter. We select

this to give us a large magnetosphere in which the middle magnetosphere region covers many grid points. The southward IMF simulation was run until a quasi-steady magnetosphere resulted. In Figure 3.3 plasma pressure and flow vectors in the dawn-dusk meridian (yz) plane (top) and equatorial plane (bottom) at a quasi-steady state for southward IMF are shown. Then a northward IMF (B_z = 0.105 nT) was imposed. Reconnection began in the plasma sheet at t = 386 hours (about 46 hours after the IMF turned from southward to northward) and a plasmoid (magnetic O-region) was launched down the tail. In Figure 3.4 we plot the location of the X- and O-lines in the tail as a function of time. When the near-Jupiter ($x = -120$ R_J) X- and O-lines formed there already was a distant X-line at about $x = -250$ R_J. By hour 390 the O-line moved to about $x = -160$ R_J. Subsequently both the X- and O-lines moved tailward. Another X/O pair formed at about t = 430 hours. This pair then retreated and a new pair formed. The period of plasmoid formation is 35 to 37 hours and the plasmoid ejection interval is from 32 to 36 hours. The average velocity of plasmoid ejection for the last three reconnection events is 444 km s^{-1} or 22.4 R_J hr^{-1} on average. The first plasmoid interacts with the pre-existing plasma sheet and distant neutral line, and then leaves the system more slowly (242 km s^{-1}). The last three reconnection events have very similar initial configurations and the plasmoids leave the system with approximately the same velocity.

In Figure 3.5 we have plotted the position of the X- and O-lines from a simulation of the Earth's magnetosphere [*Ogino et al.*, 1994]. The top panel shows the position of the neutral lines and bottom panel shows the velocities of earthward and tailward flows. Initially the simulation was run without an IMF. At t = 120 hours a northward IMF entered the simulation box and the IMF was turned southward at t = 390 hours. An X/O pair formed at about t = 450 hours (60 hours after the southward turning). Large (> 450 km s^{-1}) tailward and earthward flows occurred by t = 540 hours.

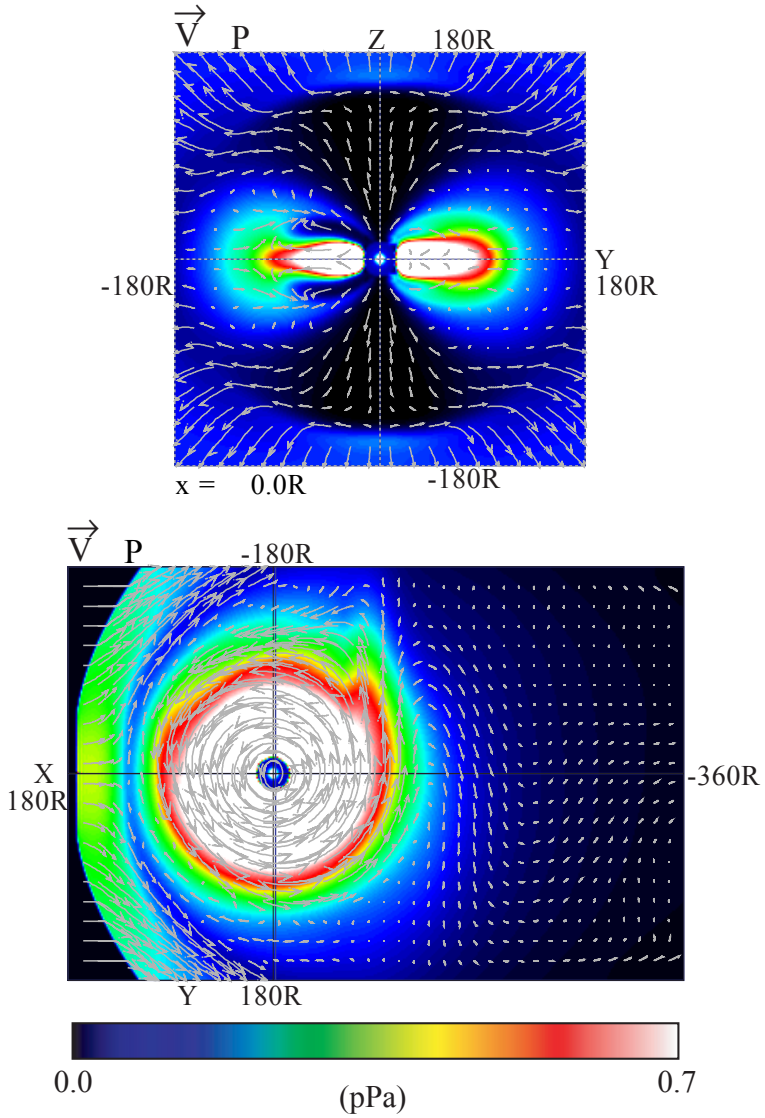

Figure 3.3: Pressure per atomic mass unit (AMU) and plasma flow vectors in the dawn-dusk meridian (yz) plane (top) and equatorial plane (bottom) for southward IMF. The solar wind dynamic pressure is 0.011 nPa and the component of IMF B_z is −0.105 nT.

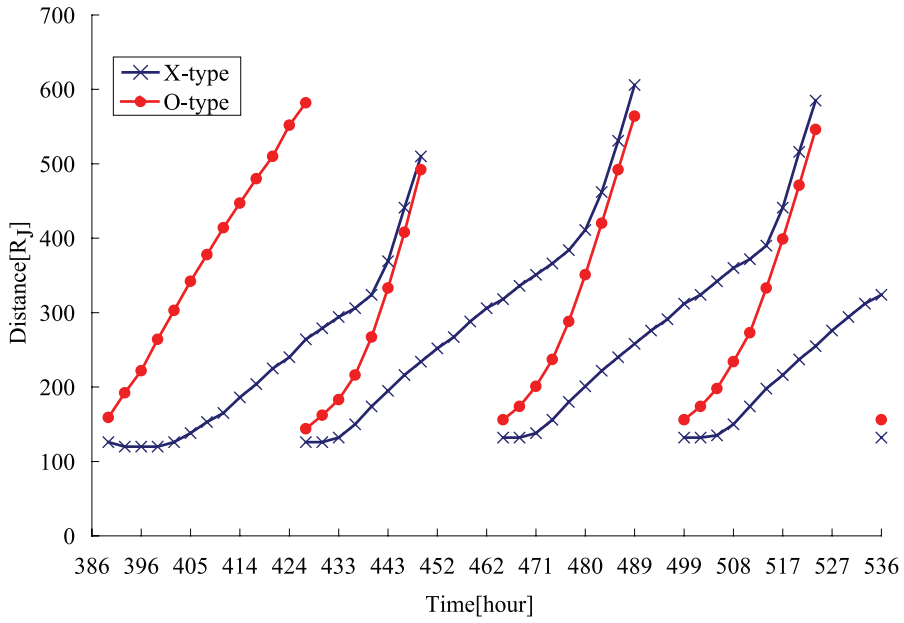

Figure 3.4: Locus of the X-type and O-type neutral lines versus time in the Jovian magnetosphere. The points are plotted every 3 hours. The slight separations in the positions of the X- and O-lines at the beginning of the events indicate that reconnection began earlier in the previous interval.

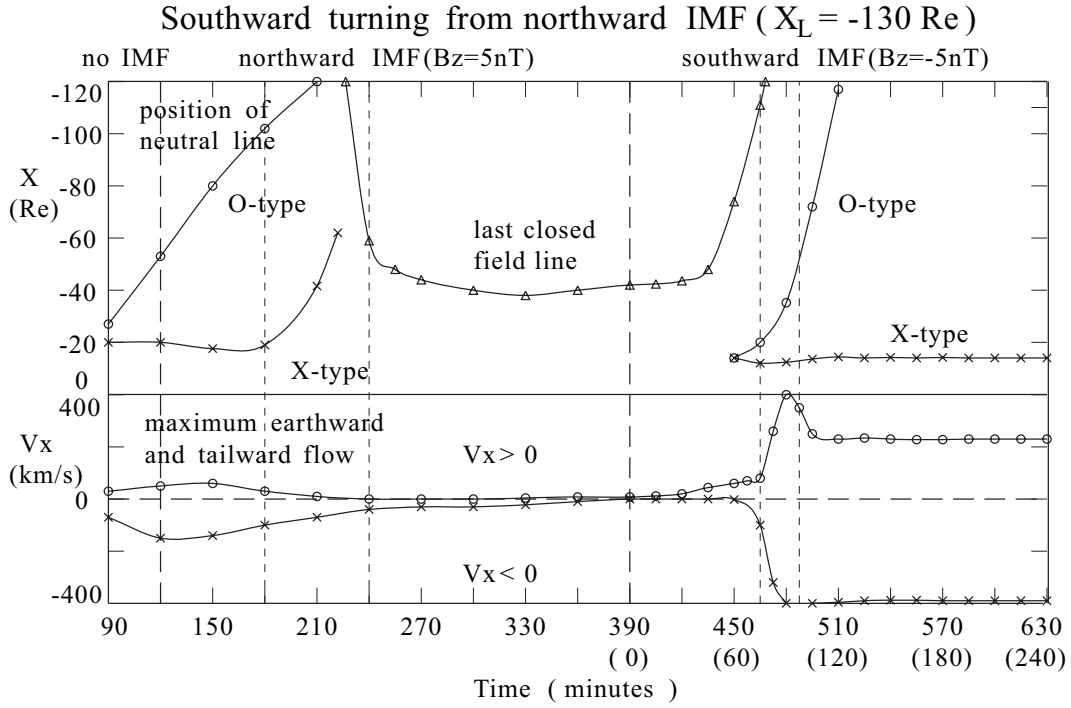

Figure 3.5: Locus of the X-type and O-type neutral lines (top) and flow velocity of earthward and tailward flow versus time in the Earth's magnetosphere (From *Ogino et al.,* 1994).

The plasmoid ejection in the Jovian magnetotail is different from that at the Earth. At Jupiter the X- and O-lines both move tailward while at the Earth the X-line stays fixed when the O-line moves tailward. In both cases the strong flow from the X-line pushes the O-line tailward. We can understand the difference between the Jupiter and Earth simulations by considering the plasma flow. At Jupiter flow from the X-line acquires rotational velocity as it moves toward Jupiter. The plasma is carried around Jupiter and then comes back to the tail. Because the rotation speed is slower than full corotation, it takes longer than one 10-hour Jovian rotation period to go all the way around Jupiter. The velocity is not purely rotational but the azimuthal component is usually largest. For instance at noon near the magnetopause the azimuthal velocity (V_Y) is 180 km s^{-1} to 240 km s^{-1} while the radial velocity (V_x) is -10 km s^{-1} to 120 km s^{-1}. The rotated plasma from the reconnection ends up back in the tail Jupiterward of the old reconnection site. In this phase, the position of the X-type reconnection line in the tail gradually moves tailward. Then, with the addition to the tail of newly opened field lines from the dayside, a new reconnection line appears in the accumulated plasma of the plasma sheet, forms a new plasmoid and ejects it tailward. This process repeats to generate periodic tail reconnection and tailward propagation of both of the O-type neutral line (plasmoid) and old X-type reconnection line. In contrast, at the Earth the plasma convects Earthward to the dayside and is carried from the dayside to the tail over the polar cap by dayside reconnection.

We have plotted magnetic field lines in the x-z plane for the interval from 465 hours to 490 hours in Figure 3.6. There are four types of field lines present. The green lines are closed field lines with both ends linked to Jupiter. Open field lines with one end at Jupiter and the other extending outside of the simulation box are magenta. Detached field lines that cross the equator twice are red, and detached field lines that cross the equator once and exit from the downstream end of the simulation box are

blue. We have divided the reconnection events into four phases. Each panel in Figure 3.6 represents one of those phases. During the first phase plasma accumulates in the tail. The snapshot at t = 465 hours was taken just as the X/O pair formed. In the second phase a small magnetic island caused by reconnection of closed field lines appears. Next, a plasmoid is ejected tailward and there is a sudden enhancement of the Jupiterward flow. During this phase lobe reconnection begins. Finally during the fourth phase the plasma flows around dawn to the dayside and then around dusk back to the nightside. The velocity of plasmoid ejection is ~495 km s^{-1} or 25 R_J hr^{-1} at 400 R_J near midnight. These four phases repeat periodically.

The magnetic field, temperature and plasma velocity in the equatorial (bottom) and dawn-dusk meridian planes at t = 478 hours are shown in Figure 3.7. Both plots give the plasma temperature as a color spectrogram with flow vectors plotted on top of the color shading. The black region near Jupiter is inside of the inner magnetosphere boundary and is not included in the calculation. In the dawn-dusk meridian plane, the plasma temperature on the duskside is higher than that on the dawnside. In the tail, the tailward flow associated with the new X/O pair pushes the previous X-line tailward (bottom). The Jupiterward flow from the X-line convects toward the dayside (bottom). At this time the O-line is ~200 R_J down the tail. It is curved toward Jupiter. The most obvious feature of Figure 3.7 (bottom) is the crescent moon shaped distribution of high temperature (A). This high temperature flow channel results from a combination of the tension on stretched dusk side field lines, the Jupiterward flow from the reconnection and atmospherically driven rotation.

In Figure 3.8 the energy flux and flow vectors have been mapped along magnetic field lines to the ionosphere. The energy flux is given by pv where p is the pressure and V is the thermal velocity. The plasma parameters were evaluated at the inner boundary of the simulation and mapped along magnetic field lines to the ionosphere.

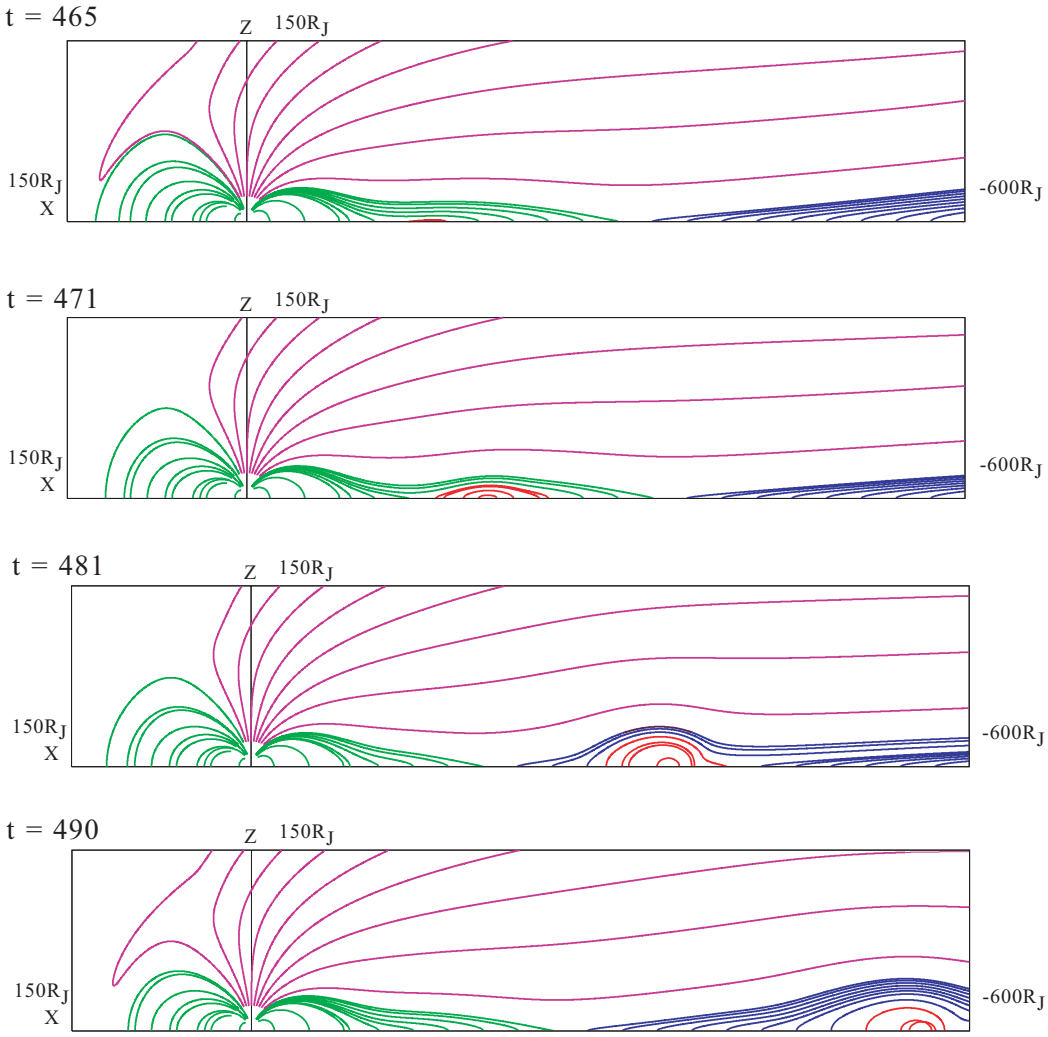

Figure 3.6: Time sequence of the configuration of magnetic field lines in the Jovian magnetosphere when a plasmoid ejects. Positive x is toward the sun, and positive z is northward. Closed field lines are shown by green, open field lines by magenta and detached field lines by red, and blue.

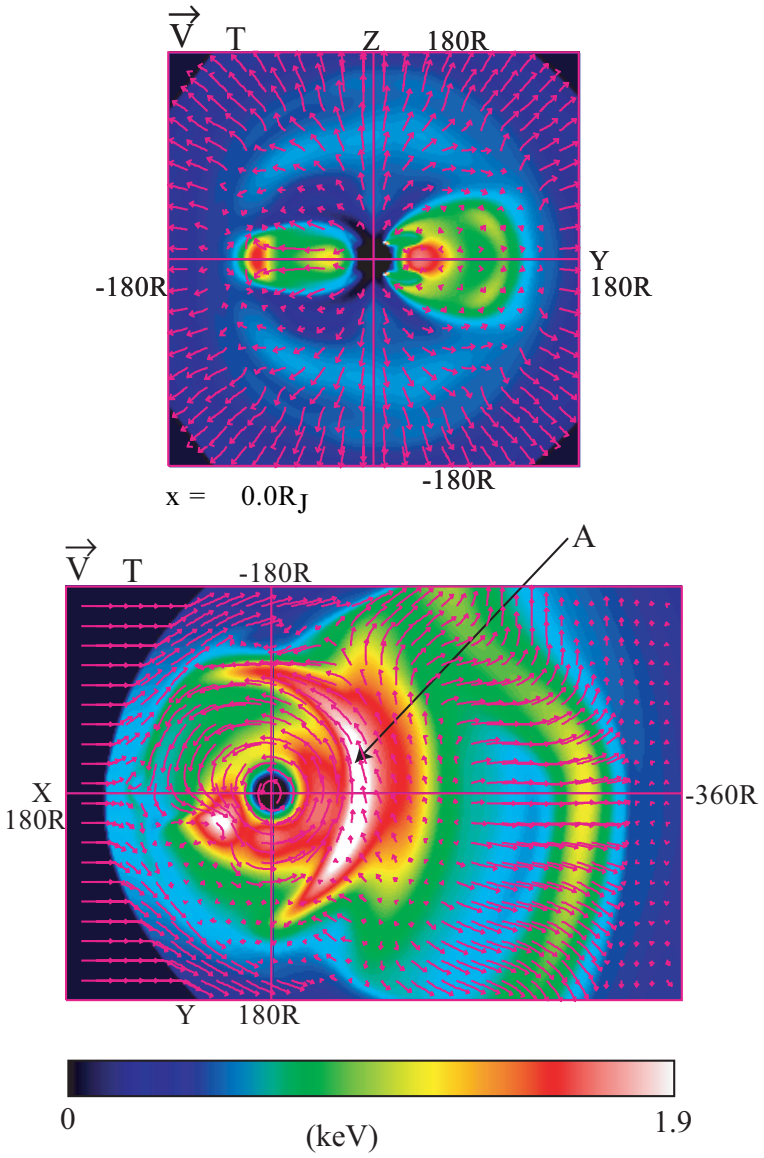

Figure 3.7: Temperature per atomic mass unit (AMU) and plasma flow vectors in the dawn-dusk meridian (yz) plane (top) and equatorial plane at t = 478 hours. The color bar gives the temperature values.

The numbers 00, 06, 12, and 18 indicate the local time (LT). In Figure 3.8 corotational flows are dominant up to near the pole. The influence of dayside reconnection can be seen by tailward flow near noon. The reconnection driven flows combine with rotation to form a large counterclockwise cell over the polar region. This dawn side cell has grown at the expense of the duskside cell. The constriction near 85^o and 15 LT, (i.e. between the dayside and duskside) is a projection of the narrow channel that starts at about 15 LT in Figure 3.7. The energy flux to the ionosphere on the duskside is greater than that on the dawnside. The area of greatest energy flux (yellow) is in between 14 LT and 16 LT.

3.3.2 Condition of Periodic Plasmoid Ejection

Here we have repeated this analysis by using seven sets of solar wind and IMF combinations: (a-VHiPHiB: very high pressure and high magnetic field) the dynamic pressure was set to 0.090 nPa and IMF was 0.420 nT, (b-VHiPLoB: very high pressure and low magnetic field) the dynamic pressure was 0.090 nPa and IMF was 0.105 nT, (c-HiPHiB) the dynamic pressure was 0.045 nPa and IMF was 0.420 nT and (d-HiPLoB) the dynamic pressure was 0.045 nPa and IMF was 0.105 nT and (e-LoPLoB) the dynamic pressure and IMF were 0.023 nPa and 0.105 nT respectively. Lastly in (f-VLoPHiB) the dynamic pressure was 0.011 nPa and the IMF was 0.420 nT. Each simulation was run for 250 hours. The simulation (g-VHiPHiB) is a special case in which the plasma density at the inner boundary was set to five times the Voyager 1 value. We found that periodic plasmoid ejection occurred for run (e-LoPLoB) and the run used for the previous subsection (marked with h-VLoPLoB) but did not occur for runs (a-VHiPHiB), (b-VHiPLoB), (c-HiPHiB), (d-HiPLoB) and (f-VLoPHiB). In runs (a-VHiPHiB), (b-VHiPLoB), (c-HiPHiB), (d-HiPLoB) and (f-VLoPHiB) quasi-steady reconnection occurred and a single plasmoid moved down the tail. In Table 3.4 we list

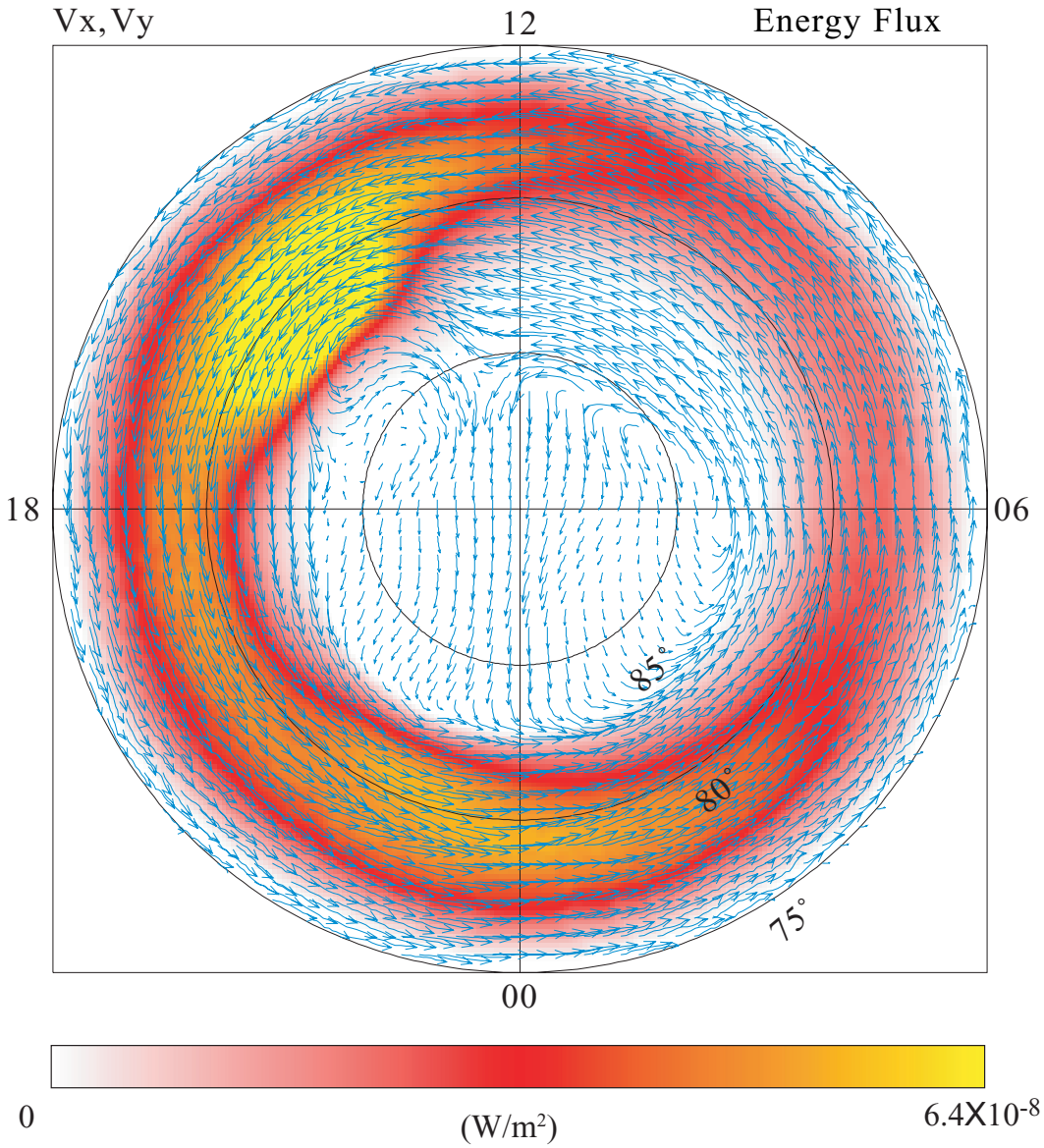

Figure 3.8: Energy flux and plasma velocity in the polar cap mapped along magnetic field lines at the same time (t = 478 hours) as in Figure 3.7. The color bar gives the value of the energy flux on a linear scale.

the locations of the sub-solar bow shock and magnetopause, the tail reconnection position at midnight and the period and velocity of plasmoid ejection as a function of solar wind pressure, IMF B_z and inner magnetosphere source strength. The distance to the reconnection line (X-line) was determined from inspection of the magnetic field and flows. The inner magnetosphere source rate was calculated by taking $\int \rho \cdot v ds$ over a surface enclosing the inner boundary of the simulation at $r = 22.5\mathrm{R}_J$.

Whether or not periodic ejections occur of X/O pairs down the tail depends on both the solar wind dynamic pressure and the magnitude of IMF B_Z. At a given B_Z the periodic ejections require a smaller dynamic pressure. For instance, in Table 3.4 periodic X- and O-lines were found in the simulation with dynamic pressure of 0.023 nPa and $B_z = 0.105$ nT (case e-LoPLoB) but not in case (d-HiPLoB) with the same magnetic field and a pressure of 0.045 nPa. Periodic X/O pairs are found for cases when the magnetopause standoff distance is largest (cases e-LoPLoB and h-VLoPLoB). Recall that the cushion region was relatively larger for smaller dynamic pressures. In Figure 3.9 we have plotted the temperature and flows from these two simulations: case (d-HiPLoB) in Figure 3.9a and case (e-LoPLoB) in Figure 3.9b. The white lines show flow streamlines. In both cases there is a neutral line at about $x \sim -120\ \mathrm{R}_J$ in the tail which drives both Jupiterward and tailward flows. Jupiterward flow from the neutral line in Figure 3.9b goes all of the way around Jupiter and returns to the tail. However, much of the Jupiterward flow in Figure 3.9a cannot move around Jupiter. Instead it joins the tailward flow in the morning region.

Our simulations with stronger dynamic pressure and larger B_Z did not produce periodic X- and O-lines if we did not increase the inner plasma rate. In order to better understand the reasons for the periodic reconnection, we ran a case with higher pressure (0.090 nPa) and magnetic field (0.420 nT) and the enhanced inner source. These solar wind parameters are the same as in case (a-VHiPHiB). This simulation gives

Table 3.4: The distance to the magnetopause (MP), bow shock (BS) and tail reconnection site (RX) along the Jupiter-Sun line and the average period of plasmoid ejections for the seven simulations in this sub section and previous sub section (h). The solar wind dynamic pressure (P_{Dyn}) and IMF B_Z conditions for the simulations as well as the plasma source rate from the inner boundary have been included. The inner source for case (g-VHiPHiB) is higher than the other cases because the plasma density at the inner boundary was set to five times the Voyager 1 value. The period is the time interval of the plasmoid ejections and the tailward velocity is the velocity of that plasmoid ejection.

	P_{Dyn} (nPa)	B_Z (nT)	BS (R_J)	MP (R_J)	RX (R_J)	Period (hour)	Inner source rate (AMU s^{-1})	Tailward velocity (km s^{-1})
(a-VHiPHiB)	0.090	0.420	88	70	-84	none	5.7×10^{30}	-
(b-VHiPLoB)	0.090	0.105	92	80	-125	none	3.9×10^{30}	-
(c-HiPHiB)	0.045	0.420	93	75	-82	none	2.5×10^{30}	-
(d-HiPLoB)	0.045	0.105	105	85	-126	none	1.5×10^{30}	-
(e-LoPLoB)	0.023	0.105	102	90	-119	56	2.0×10^{30}	238
(f-VLoPHiB)	0.011	0.420	160	91	-96	none	1.4×10^{30}	-
(g-VHiPHiB)	0.090	0.420	114	90	-75	20-50	1.7×10^{32}	328
(h-VLoPLoB)	0.011	0.105	144	117	-125	34	6.8×10^{30}	444

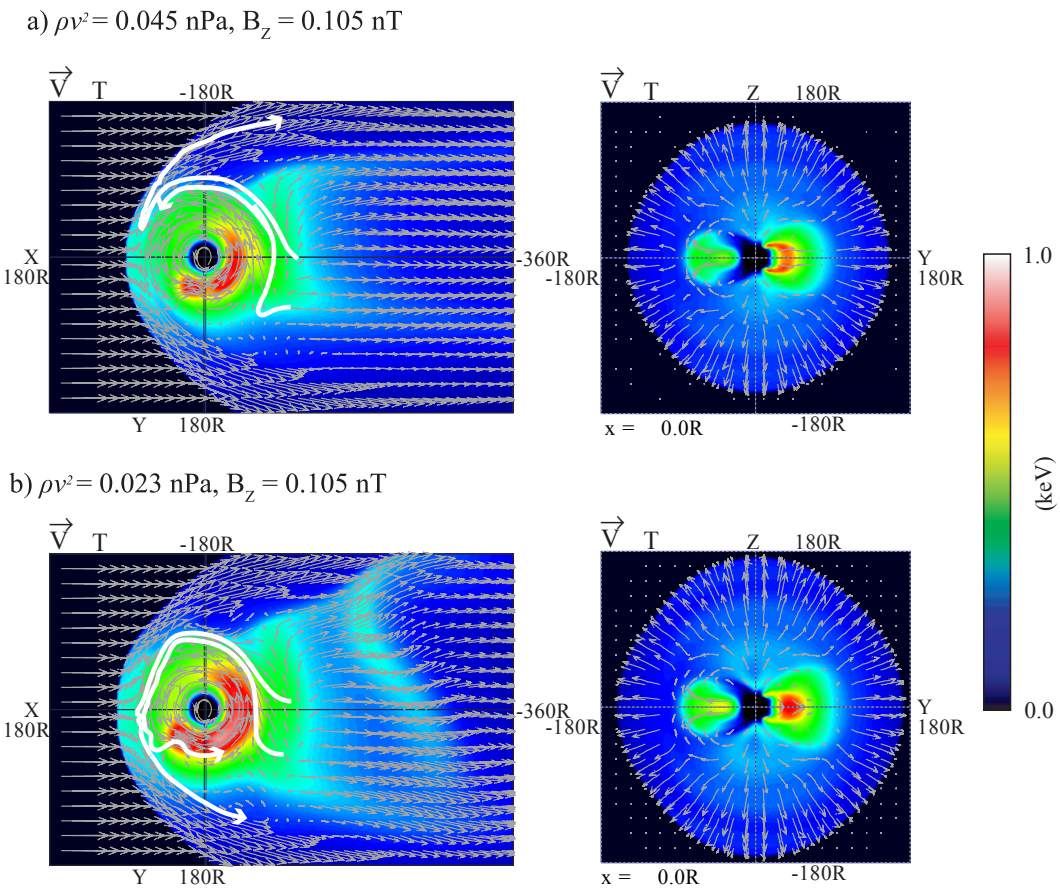

Figure 3.9: Temperature per AMU and plasma flow vectors in the dawn-dusk meridian plane (right) and equatorial plane (left). Top panel gives the results with a solar wind dynamic pressure of 0.045 nPa and 0.105 nT IMF (case d-HiPLoB) and the bottom contains the results with a dynamic pressure of 0.023 nPa and 0.105 nT IMF (case e-LoPLoB). The color bar gives the temperature values. The white lines are flow streamlines. In the top panel between dawn and noon the flow is pushed tailward by the solar wind.

an unrealistic source rate of 1.7×10^{-32} s^{-1} compared to 5.7×10^{-30} s^{-1} for case (a-VHiPHiB) but helps to demonstrate the processes that lead to periodic reconnection. In Figure 3.10 we have plotted the location of the X- and O-lines in the tail at midnight as a function of time for simulation (g-VHiPHiB). Multiple X/O pairs form in this case much, as they did for the case with $\rho v^2 = 0.011$ nPa and $B_Z = 0.105$ nT (see Figure 3.4). In this time there appear two periods associated with the reconnection: one at about 20 hours and one at about 50 hours. X/O pairs formed in the tail as early as $t \sim$ 475 hours. However they did not extend to midnight so we will start our analysis at $t =$ 538 hours. At $t = 538$ hours an X/O pair formed near-Jupiter ($x = -120$ R$_J$) and began to move tailward. After 20 hours a new X/O pair were generated at around $x = -75$ R$_J$. These also moved tailward. About 50 hours later X- and O-lines reformed at about $x = -120$ R$_J$ and repeated this sequence. In this case two X/O pairs formed every 70 hours. The average velocity of plasmoid ejection for case (g-VHiPHiB) is 328 km s^{-1} or 16.5 R$_J$ hr^{-1}. This is somewhat slower than we found in the run (h) (444 km s^{-1}) but is faster than for case (e-LoPLoB). Figure 3.11 is a snapshot of the pressure in the equatorial plane with superimposed flow vectors from case (g-VHiPHiB) at hour 544 and hour 562. At $t = 544$ hours an X/O pair has just formed at $x = -120$ R$_J$. Eighteen hours later (Figure 3.11b) this plasmoid can be seen to move tailward at $x < -300$ R$_J$ and a second plasmoid has formed closer to Jupiter and is beginning to move tailward. In the low pressure and small IMF case (h-VLoPLoB), the time between ejections was determined by the time needed for flux tubes to convect from the dayside around dusk to the tail reconnection site. In Figure 3.11a the Jupiterward flow from the X-line affects the magnetosphere in two ways. First, flow from the neutral line has pushed both the dawn and dusk tail magnetopauses outward. Second, some of the flow from the neutral line as moved around the dusk side toward the dayside moving opposite to the direction of corotation. This counter-rotating flow enhances the tendency for the dusk

side flow to form vortices (see Figure 3.2b). The result is a large scale vortex on the dusk side (circled in magenta). In the presence of this vortex, flux can return to the reconnection region much faster than if it had to convect all of the way around Jupiter and another X/O pair can form much more quickly. The second X/O pair does not drive flows around the dusk flank (Figure 3.11b) and as a result it takes longer time to set up the new neutral lines since flux tubes must convect all the way around Jupiter. In the XY plots in Figure 3.11 waves along the edges of the box can be seen. These waves are generated by the plasmoid ejection. The XY plots are the close-up plot. Scale of the simulation system is $-450\ R_J < x < 225\ R_J$, $-225\ R_J < y < 225\ R_J$ and $0 < z < 225\ R_J$. Thus in Figure 3.11 the real boundary is $45\ R_J$ from the boundary of the figure. That is why the boundary condition does not affect the periodic plasmoid ejection.

The Jovian magnetosphere settled down to a steadily reconnecting state in cases (a-VHiPHiB), (b-VHiPLoB), (c-HiPHiB), (d-HiPLoB), and (f-VLoPHiB). The cases with periodic plasmoids discussed above had $B_Z = 0.105$ nT. Two of the steadily reconnecting cases (b-VHiPLoB and d-HiPLoB) also had $B_Z = 0.105$ nT. The neutral line in these simulations was at $x \sim -125\ R_J$ (Table 3.4). In Figure 3.9a (case d-HiPLoB) the flow from the neutral line does not go around Jupiter. Instead most of the flow turns tailward. In Table 3.5 we have included the thickness of the cushion region for these simulations. It was $14\ R_J$ wide in case (d-HiPLoB). Although the dynamic pressure in case (b-VHiPLoB) was twice that in case (d-HiPLoB), the cushion region had approximately the same thickness ($15\ R_J$). In this case also most of the flow did not go around Jupiter.

Cases (a-VHiPHiB) and (c-HiPHiB) are examples when the IMF is important for determining the magnetospheric configuration in the middle magnetosphere. In Table 3.5 we have tried to isolate the effects of the IMF on the rotating flows of the middle

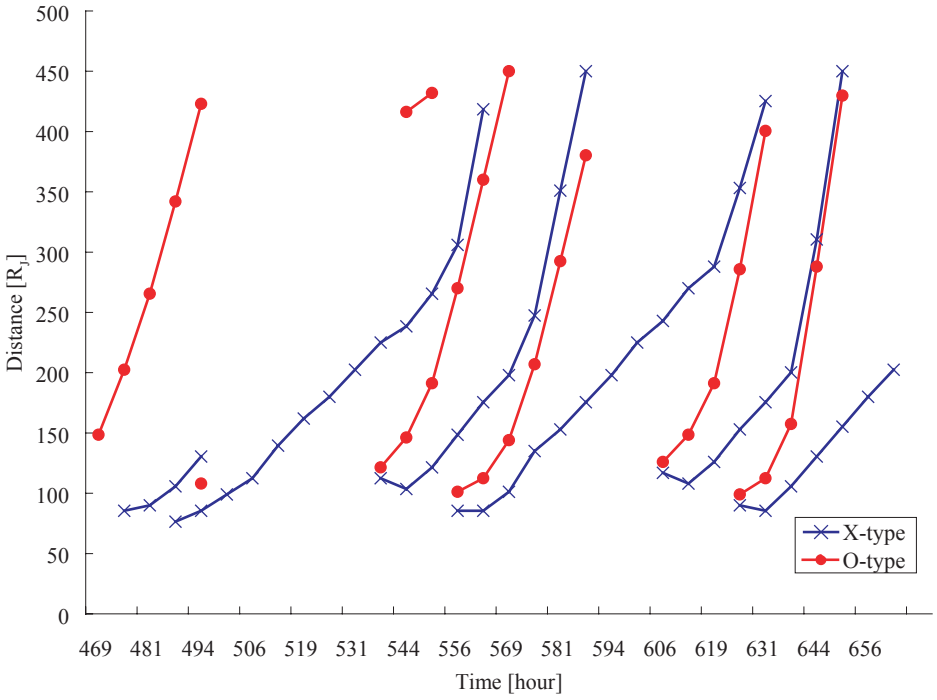

Figure 3.10: Locus of the X-type and O-type neutral lines versus time. The points are plotted every 6.25 hours. The slight separations in the positions of the X- and O-lines at the beginning of the events indicate that reconnection began earlier in the previous 6.25 hour interval. Between 494 and 544 hours the neutral lines did not extend in azimuth to midnight so that no O-line points have been plotted.

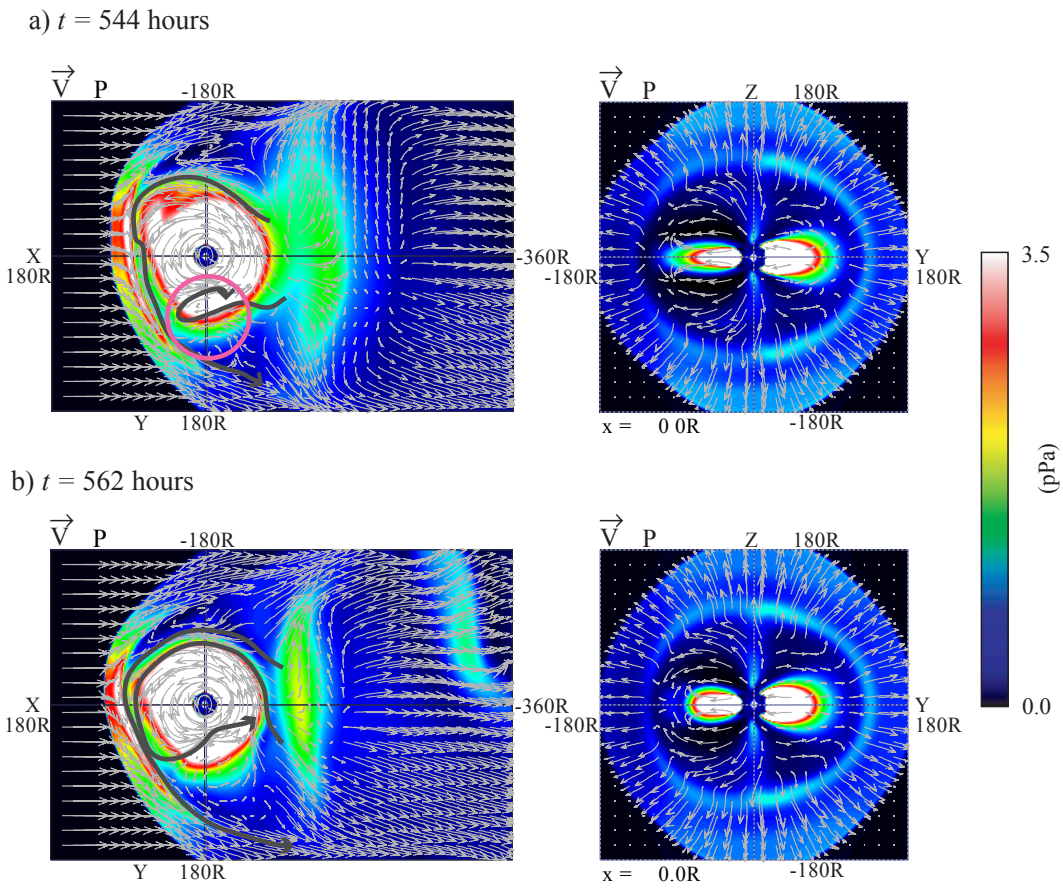

Figure 3.11: Plasma pressure and plasma flow vectors in the dawn-dusk meridian plane (right) and equatorial plane (left) with a solar wind dynamic pressure of 0.090 nPa and 0.420 nT IMF (case g-VHiPHiB). The grey lines are the flow streamlines. Top panel is the result at t = 544 hours and the bottom is at t = 564 hours. The color bar gives the pressure values. In the magenta circle the reconnected flow streams toward the dayside and then returns to the tail.

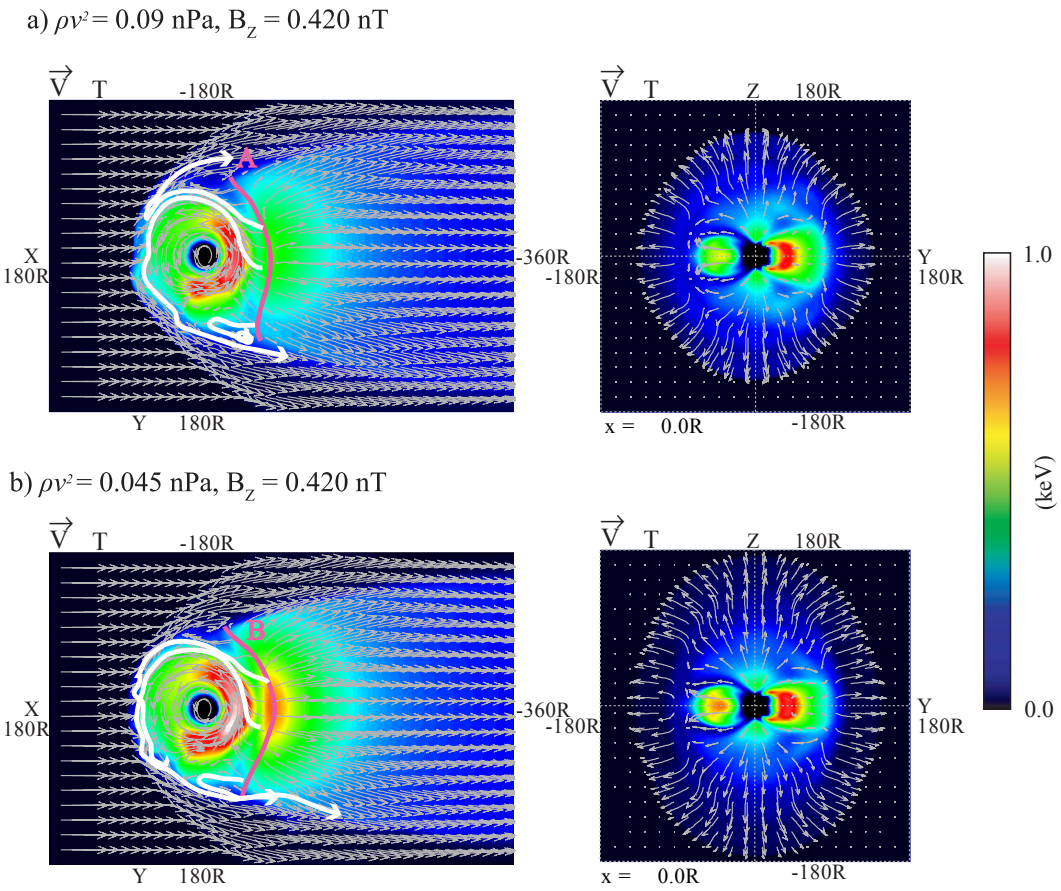

Figure 3.12: Temperature per AMU and plasma flow vectors in the dawn-dusk meridian plane (right) and equatorial plane (left). Top panel is the result with a solar wind dynamic pressure of 0.090 nPa and and an IMF of 0.420 nT (case a-VHiPHiB) and the bottom contains the results with a dynamic pressure of 0.045 nPa and IMF of 0.420 nT (case c-HiPHiB). The color bar gives the temperature values. The white lines are flow streamlines. The lines A and B indicate the neutral lines. The reconnection was quasi-steady in both of these simulations.

magnetosphere by calculating the ratio of the tail rotation boundary distance with an IMF to that without for constant solar wind dynamic pressure. This is called the compression ratio. Cases (a-VHiPHiB) and (c-HiPHiB) have the smallest ratios, indicating that reconnection is more important for determining the location of the rotation boundary in these cases. The flows and temperatures from these simulations are plotted in Figure 3.12. In Table **??** the cushion region was only 7 R_J and 4 R_J wide in these cases. The tail neutral line is at approximately -80 R_J down the tail in both cases. In these two examples the flow from the tail neutral line joins with Jovian rotational flows. Most importantly, unlike case (e-LoPLoB) the flux tubes that convect around Jupiter in cases (a-VHiPHiB) and (c-HiPHiB) do not participate in the tail reconnection again. In case (a-VHiPHiB) flow from the dawn half of the neutral line exits the dawn magnetopause (A). Flow from the duskward half of the neutral line goes around Jupiter and ends up along the dusk magnetopause. A few flux tubes convect into the tail (not marked in Figure 3.12) but they stay in the current sheet. None of the flux tubes participate in reconnection again.

3.4 Discussions

For the plasmoid ejections in the simulations, the convective flow time determines the period of X- and O-line ejections. The convective flow time in turn is determined by a combination of tail reconnection and rotation of the reconnected plasma. The solar wind, the IMF and the density of Jovian plasma influence tail reconnection and acceleration of the reconnected plasma toward corotation. The magnitude of the IMF affects the reconnection rate and the distance to the magnetopause. Most importantly it determines where tail reconnection occurs. For instance in Table 3.4 for B_Z= 0.105 nT, the tail X-line at midnight is found at $x \sim -125$ R_J for all of the simulations even

Table 3.5: The subsolar distance to the corotation region, thickness of the cushion region and ratio of the distance to the rotation boundary in the tail on the x-axis for constant solar wind dynamic pressure with an IMF to that without an IMF. The cushion region was determined by using the same method as in Table 3.3. The reconnection to rotation ratio is the distance to the neutral line in Table 3.4 divided by the corotation boundary with no IMF in Table 3.3. $X_{dayside}$, X_{tail} and X_m are the same descriptions as Table 3.3.

			Corotation boundary distance		Cushion region	Compression	Reconnection to rotation
	P_{Dyn} (nPa)	B_Z (nT)	$X_{dayside}$ (R_J)	X_{tail} (R_J)	X_m-$X_{dayside}$ (R_J)	IMF/no IMF	Reconnection /X_{tail}
(a-VHiPHiB)	0.090	0.420	63	61	7	0.68	0.93
(b-VHiPLoB)	0.090	0.105	65	86	15	0.96	1.38
(c-HiPHiB)	0.045	0.420	71	70	4	0.69	0.82
(d-HiPLoB)	0.045	0.105	71	83	14	0.82	1.25
(e-LoPLoB)	0.023	0.105	69	94	21	0.82	1.03
(f-VLoPHiB)	0.011	0.420	73	84	18	0.73	0.83
(g-VHiPHiB)	0.090	0.420	85	69	5	0.77	0.83
(h-VLoPLoB)	0.011	0.105	108	101	9	0.88	1.09

though we changed the dynamic pressure by a factor of 8.

In Figure 3.13 we have plotted the distance to the rotation boundary at midnight versus the solar wind dynamic pressure. Large black dots show the distance to the rotation boundary when the IMF was set to zero from Table 3.3 and large open dots which indicate that distance when the IMF was included from Table 3.5. In all the cases the corotation boundary moves closer to Jupiter when there is an IMF. The change is smallest for the highest dynamic pressure and smallest B_Z (case b-VHiPLoB). We also plotted with open triangles the location at which tail reconnection occurred. For the cases (e-LoPLoB and h-VLoPLoB) with periodic reconnection, the neutral line occurs close to the location of the outer edge of rotation in the absence of an IMF. However the corresponding rotation boundary with the IMF is located much closer to Jupiter. For some cases with steady reconnection (b-VHiPLoB and d-HiPLoB) the neutral line is far from either rotation boundary.

In Figure 3.14 we have sketched our understanding of the interaction between the solar wind and Jovian magnetosphere. First recall that reconnection occurs in the simulation even when there is no IMF. Flux tubes convecting into the tail around dusk are sufficiently stretched such that they reconnect (see Figure 3.2). The magnetospheric response becomes much more complex when we add even a constant northward IMF. Periodic neutral lines occur when the solar wind dynamic pressure is low and the IMF is small (cases e-LoPLoB and h-VLoPLoB). The small dynamic pressure allows the magnetopause to move away from Jupiter creating a relatively large cushion region. The small IMF leads to a tail neutral line that is far from Jupiter (1). Under these conditions flux tubes can convect from the neutral line around Jupiter and arrive back in the tail. As they convect around dusk the field lines are stretched and they can participate in reconnection again (2). The tailward flows from the second neutral line force the original X/O pair to retreat tailward (3). The old neutral line is pushed by the

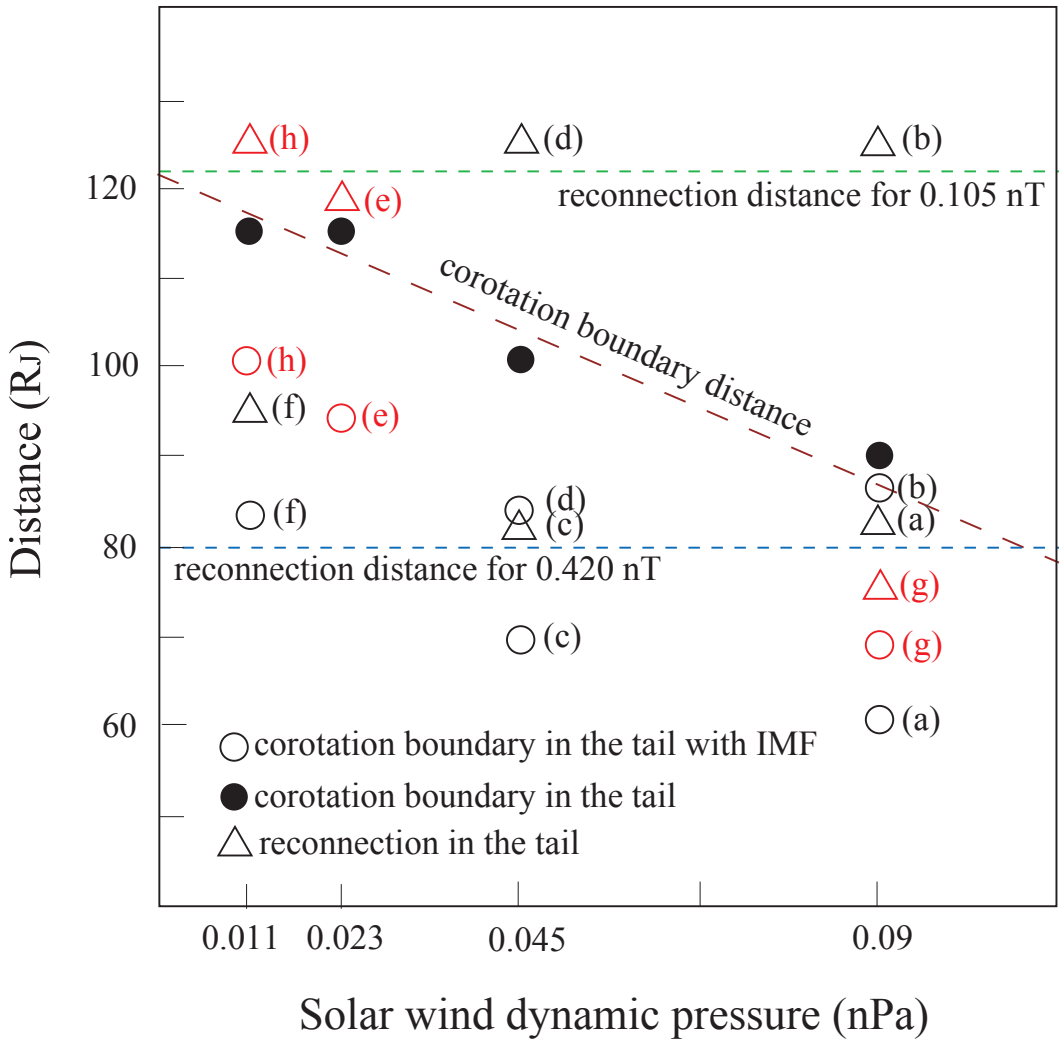

Figure 3.13: Relationship between the corotation region and reconnection in the tail. The horizontal axis is the solar wind dynamic pressure (nPa) and vertical axis is the distance from the Jupiter (R_J). The large black dots indicate the outer distance of corotation with the IMF turned off and the large open dots indicate the outer distance of corotation with an IMF. The triangles show the reconnection distances at midnight. The red colored circles and triangles represent the cases for which periodic plasmoids occurred. The brown line is the approximate line of the corotation boundary and the green line and blue lines are the approximate distances of the neutral line in the tail for 0.420 nT and 0.105 nT, respectively.

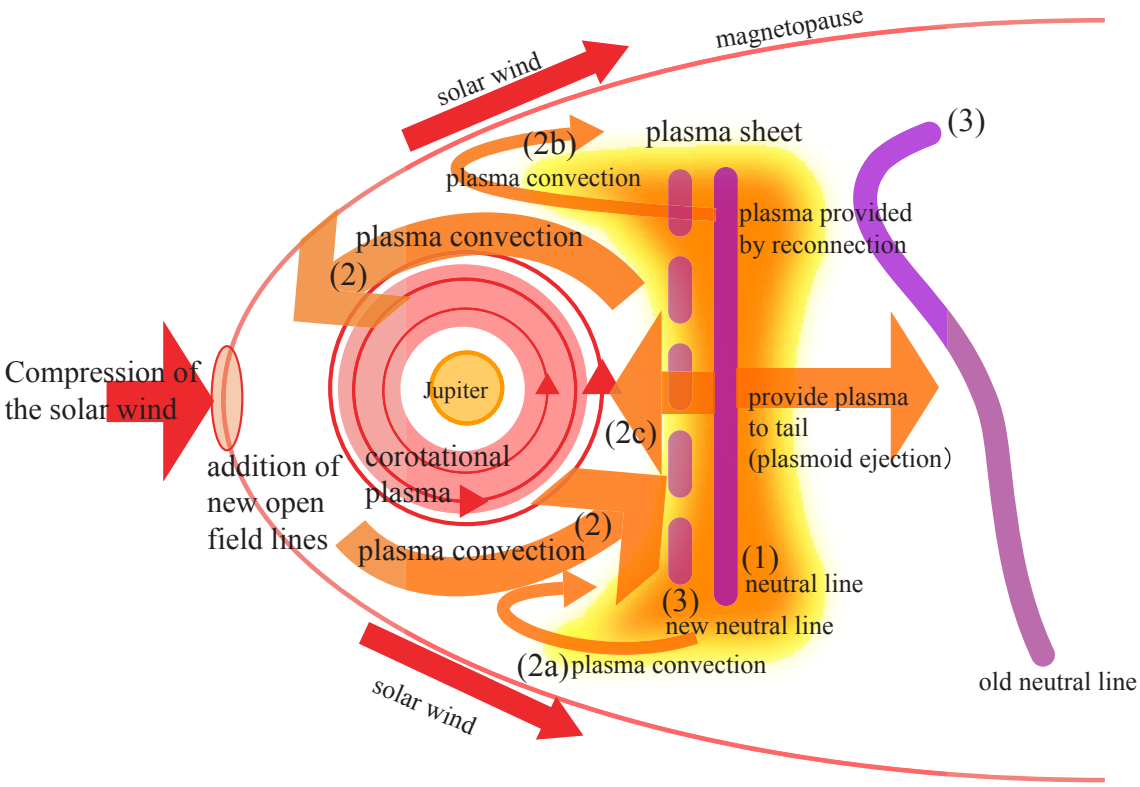

Figure 3.14: Schematic diagram to demonstrate a mechanism for plasma circulation consistent with periodic variation of Jovian magnetotail dynamics in the equatorial (xy) plane (see the text for a description).

plasmoid and shows the dawn-dusk asymmetry.

For small IMF strength, increasing the dynamic pressure compresses the day-side magnetopause while the neutral line stays in place (e.g. cases c-HiPHiB and d-HiPLoB). In these cases the flow from the neutral line cannot go all the way around Jupiter. Instead the flow direction reverses near dawn and the flux tubes convect down the tail (Figure 3.9a). This is sketched in path 2b (Figure 3.14). When the IMF is larger, the neutral line forms closer to Jupiter (cases a-VHiPHiB and c-HiPHiB). The Jupiterward flow compresses the rotating plasma disk (2c). The flux tubes from the reconnection move around Jupiter but most of the flux tubes stay on the dusk flank and do not penetrate towards the central part of the plasma sheet. Thus they do not participate in reconnection again. For these cases the reconnection in the tail is steady.

Case (g-VHiPHiB) with its extreme plasma source demonstrates the importance of returning flux to the tail in creating the periodic reconnection. In this case there were two periodicities in the reconnection. One period was determined by the convection around Jupiter while the second shorter period is caused by a flow vortex in the dusk region like path 2a in Figure 3.14. This vortex allowed flux tubes to return to the tail more quickly.

Tailward and Jupiterward flow bursts in the early morning quadrant were observed by the Galileo Energetic Particles Detector (EPD) to reoccur every 48 to 72 hours [*Woch et al.*, 2002]. It is tempting to associate these flow bursts with the periodic formation and retreat of X- and O-line pairs. The periods in our simulation (34 - 56 hours) are somewhat lower than the observed timing of the bursts. In the simulation the X- and O-lines form at $x \sim -120$ R_J. Galileo observed the flow bursts at distances of 95 R_J - 125 R_J in the tail and the flow bursts were both Jupiterward and tailward [*Woch et al.*, 2002]. Thus the X-line in the simulation is in the region of the observed flow reversals. The average dynamic pressure observed at Jupiter is 0.1 nPa and the

average IMF is 0.8 nT [*Joy et al.,* 2002]. The dynamic pressure (0.011 - 0.090 nPa) and the magnitude of the IMF (0.105 - 0.420 nT) used in the simulation was lower than that typically observed. In this simulation the IMF was held northward for a long time (up to 250 hours). The IMF observed on Voyager 2 near Jupiter kept one sign of B_Z for one week and intervals with one sign for 3 or 4 days have been often observed [*Walker et al.*, 2001]. However, usually the IMF varies on shorter time scales. In addition the IMF usually has x and y components in addition to B_Z. The plasma ejection period may be longer when the Jovian magnetosphere is simulated under more ordinary IMF conditions. Recently *Kronberg et al.* [2005] have reported these flow bursts and new interpretation. Our simulation results are consistent with *Woch et al.* [2002] in the respect of the IMF effects. *Kronberg et al.* [2005] say that the flow burst occurs by the internal processes and the IMF does not play an important role so much. We have the simulation result which reconnection occurred for no IMF (see Figure 3.2). Thus the changing of solar wind dynamic pressure may lead to the behavior as their similar to that in model but we have not yet found the periodic ejections under the changing the dynamic pressure. Also there is no other Jupiter's simulation model to occur the periodic plasmoid ejections.

3.5 Summary

We have used a series of simulations of the interaction of the Jovian magnetosphere with the solar wind to investigate the influence of the IMF and magnetic reconnection on the magnetospheric configuration. First we investigated at the simplest cases in which the IMF was set to be zero. In these calculations we was interested in determining the effects of dynamic pressure changes on the rotating equatorial plasma sheet and on the size of the cushion region that separates the plasma sheet from the dayside

magnetopause. The dynamic pressure controls the overall size of the Jovian magnetosphere. It also determines the location of inertial reconnection in the tail. When the dynamic pressure is large, the cushion region becomes relatively thin, and changes in the pressure directly affect the plasma sheet but when the dynamic pressure is smaller, the cushion widens and it absorbs most of the pressure change without affecting the plasma sheet.

Next we added a northward IMF and performed a number of numerical experiments by changing both the dynamic pressure and the IMF strength. We found that both dynamic pressure and the IMF influence the response of this rapidly rotating magnetosphere. In particular the magnitude of IMF mostly controlls the location of tail reconnection. The position of the tail neutral line in turn determines how the reconnection generated flows interact with the rotating plasma sheet. For small pressures and IMF, tail reconnection becomes periodic. In these cases the neutral line forms far from the outer edge of the rotating plasma sheet. Flux tubes generated by tail reconnection can convect completely around Jupiter and return to the tail. When they reach the tail and accumulate there, the magnetic field become stretched and can reconnect. The new X/O pair forces the original X/O pair to move down the tail away from Jupiter. When the dynamic pressure and IMF are larger, the tail reconnection becomes steady. In some cases the flow from the reconnection reverses near the dawn magnetopause and returns tailward. If the reconnection driven flows are strong enough and the neutral line is near enough, the Jupiterward flow from the neutral line compresses the plasma sheet. In these cases the reconnected flux tubes rotate around Jupiter but exit along the dusk flank and do not reconnect again.

The periodicity of our simulation results were slightly shorter than that of the observed similar flow burst. In these simulations, the value of the solar wind dynamic pressure and northward IMF were set to lower than the obseved mean values and this

may make the difference between the period of simulations and observations.

Chapter 4

Magnetospheric Convection at Saturn as a Function of IMF B_Z

4.1 Kronian Simulation Model

Our Kronian simulation model is based on the code developed for Jovian magnetosphere [*Ogino et al.*, 1998] and almost same as described in Chapter 3. In this section we briefly review the simulation model and show how this calculation differs from previous calculations. Starting from a model of the plasma and field configuration near Saturn, we placed an image dipole upstream of Saturn at time $t = 0$. We launched an unmagnetized solar wind with a dynamic pressure of $\rho v_{sw}^2 = 0.0083$ nPa ($v_{sw} = 300$ km s^{-1}) and a temperature of 2×10^5 K from the upstream boundary of the simulation box and solved the normalized resistive MHD equations as an initial value problem by using the Modified Leap Frog Method described by *Ogino et al.* [1992]. Published values of the solar wind dynamic pressure near Saturn range from 0.0002 nPa to > 0.045 nPa [*Slavin et al.*, 1985; *Crary et al.*, 2005]. Since the higher values occurred during corotation interaction regions (CIRs) we selected a value near the lower end to

represent less disturbed times.

The Kronian magnetosphere was modeled on a 602 × 402 × 202 point Cartesian grids with a grid spacing of 0.3 R_S (1 R_S = 60,040 km), thus the simulation domain covers the region, $-120 < x < 60$ R_S, $-60 < y < 60$ R_S, $0 < z < 60$ R_S. In the simulation the magnetic field (**B**), velocity (**v**), mass density (ρ) and thermal pressure (p) are maintained at solar wind values at the upstream boundary. Symmetry boundary conditions are used at the equator ($z = 0$) while free boundary conditions are used at the top, sides and downstream boundaries. **B**, **v**, ρ and p at the inner boundary ($r < 5$ R_S) are determined from a static equilibrium in which gravity, pressure gradients, rotational forces and magnetic forces are in balance. At the inner boundary the parameters are fixed to those from the equilibrium. The simulation quantities are connected with the inner boundary through a smooth transition region ($5 < r < 6.5$ R_S). The magnetic field is directed oppositely to that at Earth. The initial plasma distributions come from the hydrostatic equilibrium as our Jupiter simulation [*Ogino et al.*, 1998]. The parameters in this hydrostatic equilibrium were set to the solar wind values at the distance where the solar wind pressure and Kronian magnetic pressure balance. The normalization factors for **B**, **v**, ρ and p are given by the dipole magnetic field, the Alfvén velocity at the planetary surface v_A= 4,359 km s^{-1}, the plasma mass density of the ionosphere ρ_s= 1.67 $\times 10^{-17}$ kg m^{-3} and the pressure at the planetary surface $p_S = 3.19 \times 10^{-4}$ Pa. For simplicity we used 20,000 nT for the main dipole (g10) rather the Cassini value of 21,084 nT [*Dougherty et al.*, 2005]. This makes an 8nT difference at the inner boundary of the simulation.

Cassini observations indicate that the plasma is mostly H_2O^+ around the moon Enceladus at $r = 4.89$ R_S and that mass flux rate from Enceladus is 3.0×10^{27} H_2O s^{-1} or 5.4×10^{28}AMU s^{-1} [*Tokar et al.,* 2006]. The source rate through a surface at 7 R_S in our simulation is 1.1×10^{28} H_2O s^{-1} or 2×10^{29}AMU s^{-1}.

4.2 Magnetospheric Convections for IMF Conditions

In addition to modeling of the Kronian magnetosphere without an IMF, we included runs with southward and northward IMF. We first ran without an IMF for 25 hours and then added a southward IMF and ran the simulation for 25 hours. Finally we fixed the IMF direction northward for 40 hours. My primary reason for keeping the IMF constant for long intervals is to obtain a quasi-steady magnetosphere. However long intervals during which the north-south component has one sign are common at Saturn's orbit. For instance during May 2004 (just before Cassini Saturn encounter) there were four intervals with more than 25 hours with one sign of B_Z and four more with more than 20 hours. The IMF magnitude is 0.4 nT which is consistent with that observed [*Ness et al.*, 1981].

In Figure 4.1 we plot the distribution of plasma mass density and velocity at location along the X-axis (left panel) and Y-axis (right panel). On the x-axis plot the y-component of the velocity (V_y) is shown while the x-component (V_x) is on y-axis plot. The results with no IMF are given by the green dashed line. The red dotted line gives the results for northward and blue solid lines show the results for southward IMF. In the case without an IMF r_{bs} = 28.9 R_S and r_{mp} = 21.4 R_S. The ratio of the magnetopause distance to the bow shock distance $r_{mp}/r_{bs} \sim 0.74$ is the same as that at Earth but is less than that at Jupiter, $r_{mp}/r_{bs} \sim 0.84$ [*Ogino et al.,* 1998]. This indicates that the magnetopause obstacle is blunter at Saturn than at Jupiter. The positions of the bow shock and magnetopause along the Sun-Saturn line are nearly the same for all three simulations (r_{bs} = 28.6 - 29.8 R_S, r_{mp} = 21.4 - 21.7 R_S). The IMF has very little effect on the position of the boundaries. At Saturn the subsolar boundaries may be controlled by the solar wind dynamic pressure and not the IMF. We confirmed this by running the zero IMF case with the dynamic pressure cut in half, and doubled. The changes in

the boundary position were r_{bs} = 26.0 - 36.8 R_S and r_{mp} = 19.3 - 25.5 R_S. The magnetopause position changes with dynamic pressure as $P_{dyn}^{-0.20}$. The subsolar Kronian magnetopause varies more with dynamic pressure than that at the Earth ($P_{dyn}^{-0.17}$) but slightly less than at Jupiter ($P_{dyn}^{-0.21}$). The variability in our simulations are larger than that of *Slavin et al.* [1985] ($P_{dyn}^{-0.16}$). At Earth the subsolar bow shock is very insensitive to the IMF while changing the IMF from 5 nT northward to 5 nT southward makes the magnetopause position vary by about 10% [*Ogino et al.,* 1992, *Walker et al.,* 1993]. At Jupiter both the subsolar bow shock and magnetopause positions change by about 10% when we rotate the IMF from southward to northward [*Walker et al.,* 2001, *Fukazawa et al.,* 2006]. At dawn and dusk the effect of changing the IMF is much larger (r_{bs} = 51.0 - 57.3 R_S, r_{mp} = 26.1 - 32.4 R_S) (Figure 4.1). A similar effect is found at Jupiter [*Walker et al.* 2005; *Fukazawa et al.*, 2006]. Both at Saturn and Jupiter this effect is much more pronounced than at the Earth. Cassini entered Saturn's magnetosphere between 0700 LT and 0800 LT. It encountered the bow shock several times between 40 R_S and 49.2 R_S and the magnetopause between 30.6 R_S and 34 R_S [*Dougherty et al.,* 2005]. The simulated magnetopause positions are in the range observed while the simulated bow shock is further from Saturn.

Figure 4.2 shows the plasma temperature and flow in the equatorial plane for the three cases. The cross section at x = 0 also is shown for northward IMF. These plots give the plasma temperature as a color spectrogram with flow vectors plotted on top of the color shading. The black region near Saturn is inside of the inner magnetosphere boundary and is not included in the calculation. In the case with no IMF, the Kronian magnetosphere demonstrates large scale vorticity. In particular a vortex is generated on the dawn side by the velocity shear between the corotation flow and the solar wind (Figure 4.2a). In this region the plasma temperature is high due to the compression of the rotating flow region by the solar wind. Additional vorticity can be seen through-

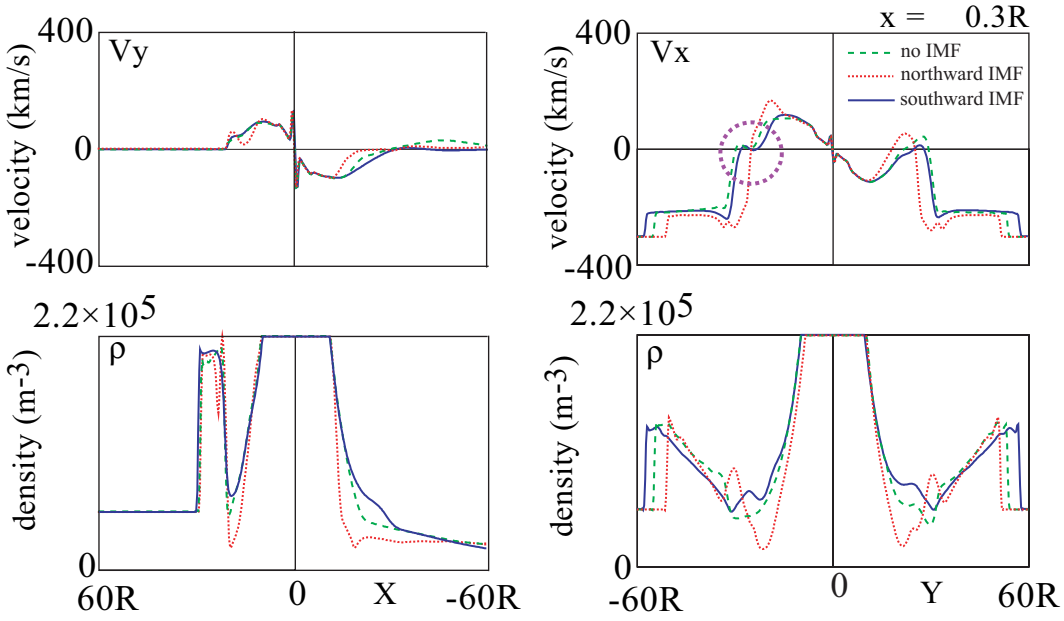

Figure 4.1: Distribution of the plasma density and velocity. Left panel shows the distribution on the X-axis and right panel is that on the Y-axis. The upper left panel contains the velocity in the y-direction and upper right panel gives that in the x-direction. The case without an IMF is plotted with the green dashed line. The red dotted line is from the northward IMF simulations and the blue solid line is from the southward IMF case. The magenta circle indicates the region of the velocity shear at dawn.

out the tail. These vortices always start in the morning (~06 LT local time, marked A) and move tailward along the magnetopause. *Galopeau et al.* [1995] investigated the occurrence of the Kelvin-Helmholtz (KH) instability at Kronian magnetopause by using observations of kilometric radiation and concluded that the KH instability tends to occur in the morning. For the no IMF case the dawn side vortices form where there is large velocity shear and relatively small magnetic shear consistent with KH waves. An examination of the time development of the general vorticity in the tail suggests that it originates with the dawnside vortices. There is no evidence of reconnection in Saturn's tail without IMF. This contrasts with simulations of the Jovian magnetosphere in which field lines in the morning tail can reconnect due to inertial effects [*Ogino et al.*, 1998].

Tail vorticity also occurs when the IMF is southward (Figure 4.2b). While the KH instability may also occurr for $B_Z < 0$, the dawn cell is much less pronounced. Southward IMF drapes the Kronian magnetosphere and reconnection occurs near $y = 0$ at high latitudes tailward of the polar cusp. This causes plasma to move from the dawn and dusk flanks of the tail toward midnight. The vortex at about $x = -40$ R_S is caused by the interaction of this flow towards midnight and the rotating flows (B). This region from 00 LT to 07 LT contains a band of high temperature plasma. Similar vortices are not seen in the results from simulations of the Earth [*Walker et al.*; 1993; *Ogino et al.*, 1994] and vorticity in Jupiter's tail is much less pronounced [*Walker et al.*, 2001; *Fukazawa et al.*, 2006].

Figure 4.2c contains results from the northward IMF case. This case is much more ordered than the other two. The dominant feature in the tail is a neutral line whose effects can be seen in the flow reversal near midnight at $x = -20$ R_S. Three vortices have formed just dawnward (C) and duskward (D and E) of the flows toward Saturn from the neutral line. The single cell near dawn forms where the flow from the neutral

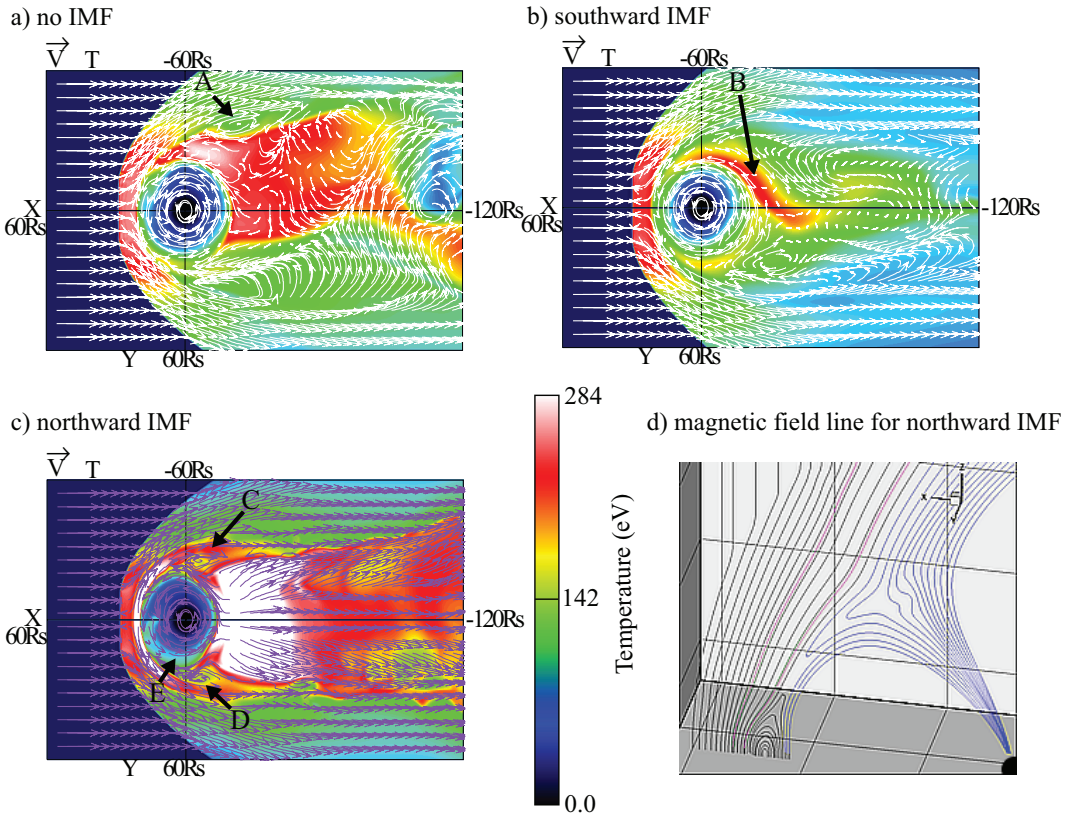

Figure 4.2: The temperature and flow vectors in the equatorial plane for the simulation with no IMF (a), southward (b) and northward IMF (c). The temperature per atomic mass unit (AMU) in eV is given by the color spectrogram. The black region in the center of the panels is inside the inner boundary of the simulation at 5 R_S. The lower right panel (d) contains magnetic field lines along the Sun-Saturn line for the northward IMF case to show a magnetic island formation at the dayside magnetopause.

line and the corotation flow are opposite to the magnetosheath flow. Near dusk cell D forms where the reconnection flow is opposite to the magnetosheath flow. The second dusk cell occurs nearer Saturn where the reconnection flow is opposite to corotation (E). This can also be seen in the red curve of Figure 4.1. The dawn cell forms in the circled region of strong shear while the two dusk cells appear as a positive peak in V_X at about $y = 20$ R_S.

All three simulations of the Kronian magnetosphere have convection vortices in the tail region. For large velocity shear and small magnetic shear at the magnetopause (no IMF and $B_Z < 0$) the vortices in the tail are nearly perpendicular to the magnetic field. This is consistent with the KH instability. The velocity shear between the corotating plasma and the solar wind is largest at dawn (δv = 300 - 440 km s^{-1}) (see Figure 4.1). This is where vortices for the case with zero IMF are likely to be generated. For southward and northward IMF the formation of flow vortices is more complex because of cusp and tail reconnection respectively. For northward IMF there is velocity shear at both dawn and dusk and vortices form on both sides.

4.3 Discussions

Two features stand out in our simulations of the Kronian magnetosphere. First, the subsolar magnetopause and bow shock positions are insensitive to the IMF and reconnection. Second, vortices formed in all three cases. They were confined to the inner magnetotail for northward IMF but were found throughout the tail for southward IMF and the case without an IMF.

To examine the effect of IMF B_Z on auroral emissions we mapped the energy flux with plasma flow vectors (upper panel of Figure 4.3) and field-aligned currents (FACs) (lower panel) to the ionosphere. The parameters were mapped along magnetic field

lines from the inner boundary of the simulation to the southern ionosphere. The vectors indicate the plasma flow and the energy flux is given by pv where p is the thermal pressure and v is thermal velocity. The FACs were calculated by taking $\nabla \times \mathbf{B}$. Red indicates downward currents and blue upward currents. We assumed the conductivity of the ionosphere was constant in the current mapping and assigned it a value of 1S. In analogy with the case at Earth we used the energy flux as a proxy for diffuse aurorae and the upward parallel currents as a proxy for discrete aurorae. The numbers 00, 06, 12 and 18, indicate the local time. We mapped to the southern hemisphere in order to compare the simulations with HST observations during January 2004. The energy flux in (a) is from the case with no IMF and the results from the southward/northward IMF simulations are shown in (b) and (c) respectively.

For the case without IMF the energy flux is high from 03 LT to 18 LT with the largest energy flux in the morning. This morning energy enhancement maps to the region with high temperature at dawn in Figure 4.2a. The high flux region is mostly located at latitudes above $75^{o}_{.}$ The energy flux in Figure 4.3a can be compared with HST auroral images in *Badman et al.* [2005]. The distribution of enhanced energy flux in Figure 4.3a should be compared with their Figures 2a and 2b since the IMF inferred from Cassini observations at this time was very small (see *Badman et al.* [2005] Figure 1). The observed auroral intensity was high between 06 LT and 12 LT and the latitude of the aurora was similar to that of our simulated energy flux enhancement. The simulated FAC are very small on the dayside in the region where the auroral emissions were found in the HST images (Figure 4.3a bottom). Only the energy flux is enhanced in this region. This suggests that the emissions observed by HST may be similar to diffuse aurorae at Earth.

For purely southward IMF the energy flux becomes more symmetric. While the dawn side energy flux is still larger than that on the dusk side the difference is smaller.

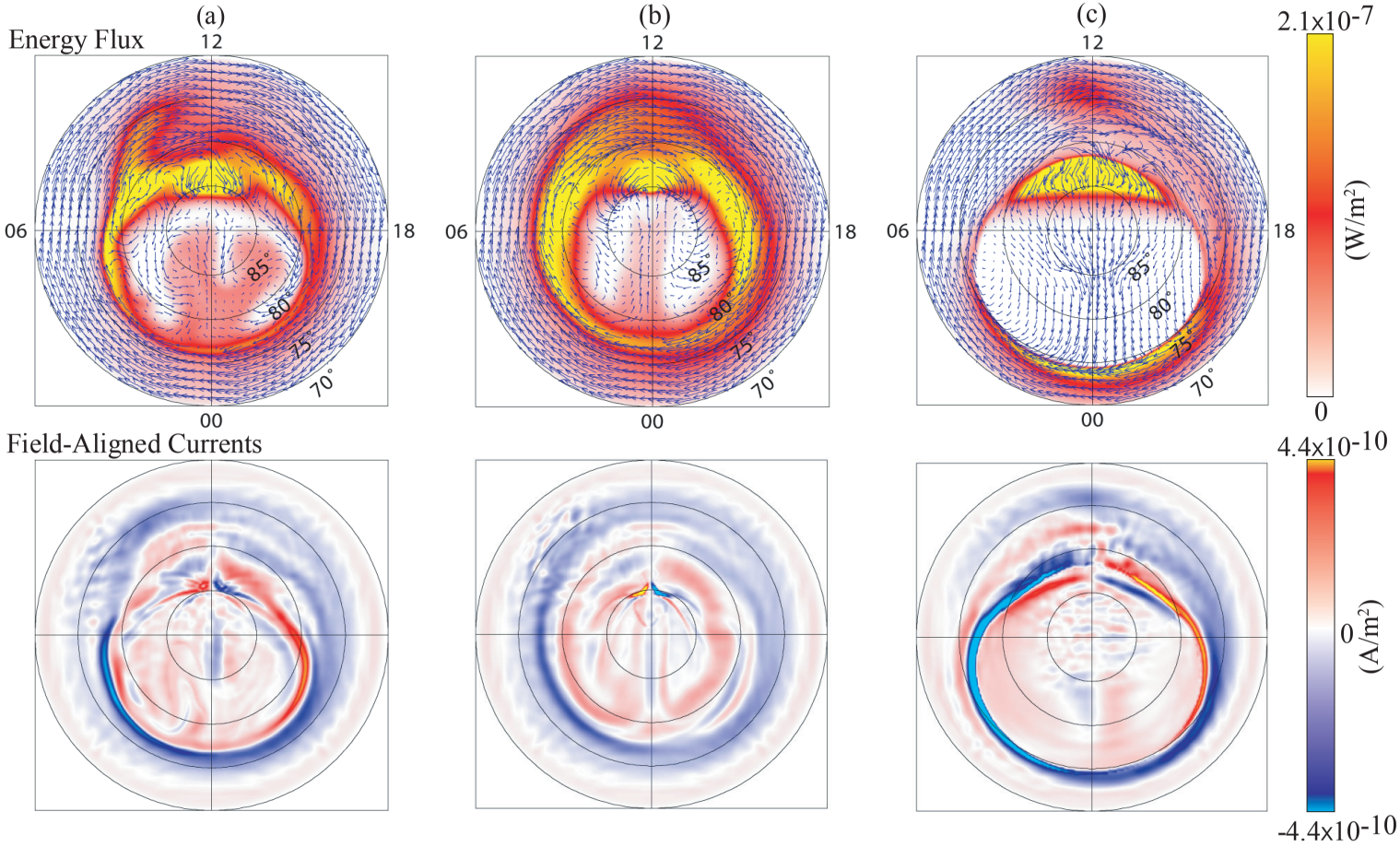

Figure 4.3: Energy flux and plasma velocity in the polar cap mapped along magnetic field lines from the inner boundary of the simulation to the southern ionosphere at the same time as in Figure 4.2 (top). The color bar gives the value of the energy flux on a linear scale. The bottom panels give the field-aligned currents with blue representing the upward (away from Saturn) currents and red downward currents. The deeper colors indicate higher current densities. Light blue and yellow are the highest currents. The value of the currents is proportional to the Pederson conductance and here we set it to 1 S to understand the rate of variation easily.

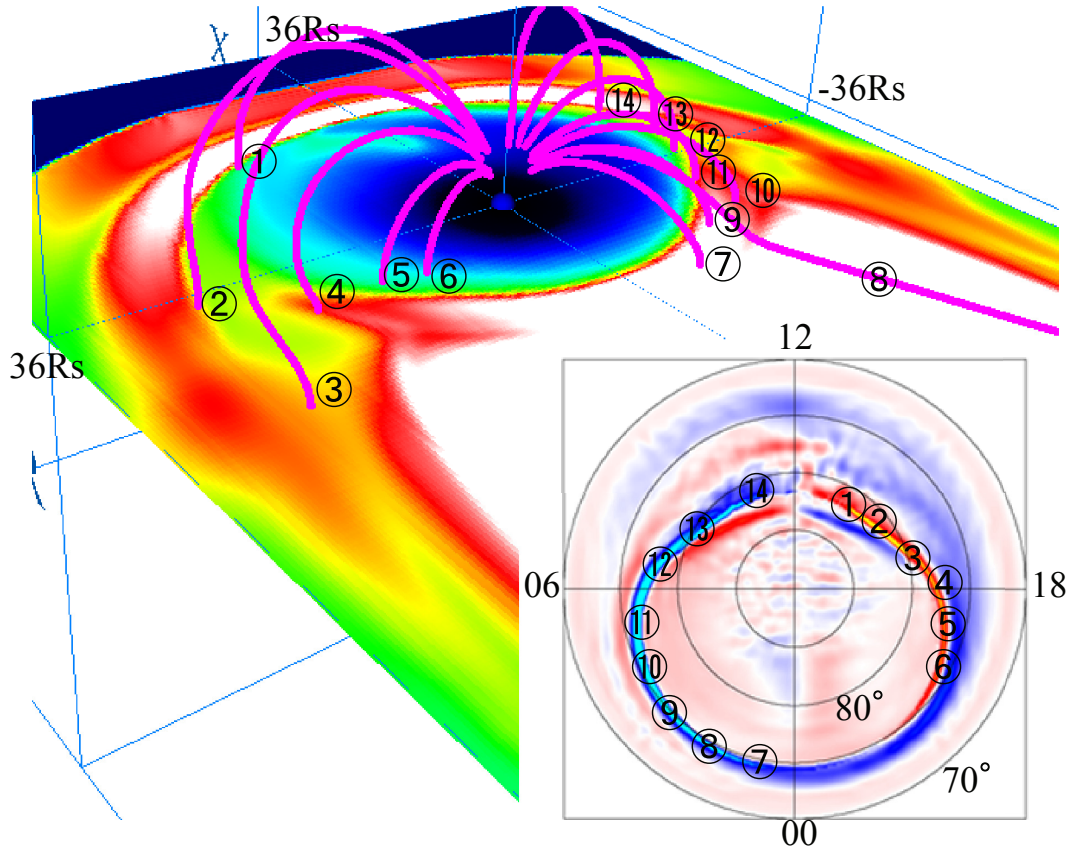

Figure 4.4: The magnetic field connection from the polar region to the magnetosphere in the north hemisphere. The picture of the equatorial plane comes from Figure 4.2 (c) and gives the temperature. The polar distribution of FACs is from Figure 4.3 (c). Magnetic field lines are magenta. The numbers from 1 to 14 show where the magnetic field maps between the polar ionosphere and the equator. The polar plot shows the southern hemisphere, so dawn-dusk are inversed when compared with equatorial plane viewed from the north.

The main difference results from the band of hot plasma near dawn (B) in Figure 4.2b. For both the no IMF and southward IMF cases there are energy fluxes and weak field-aligned currents at high latitudes in the “polar cap”. These are related to the vorticity and plasmas in the distant tail.

When the IMF is northward reconnection at the equatorial magnetopause opens field lines and the polar cap enlarges. For this simulation the region with the largest energy flux is in the polar cusp. If we compare Figure 4.3b and c both the energy

flux and field-aligned currents in the polar cusp are largest for northward IMF. Thus in the simulations the cusp emissions are strongly influenced by the IMF, as suggested by *Bunce et al.* [2005]. The dawnside upward field-aligned currents are strongest for northward IMF. The maximum upward/downward currents come from the small vortices on either side of the neutral line in Figure 4.2c. This can be seen in Figure 4.4 where we have reproduced the temperature spectrogram from Figure 4.2c and mapped the parallel currents along field lines into the magnetosphere. Recall that the current plot was in the southern hemisphere while we are looking at the equator from the north. The strong dawn side upward currents (7-14) map to the dawn side vortex while the strong dusk side downward currents (1-6) map to the dusk side vortex. *Cowley et al.* [2004] noted that the increased vorticity at dawn can lead to enhanced aurorae which is consistent with the simulations.

In Figure 4.1 there was no erosion of the subsolar magnetopause for northward IMF; yet reconnection occurred in the tail and drove flows both toward and away from Saturn (Figure 4.2). In Figure 4.2d we have plotted field lines near the subsolar magnetopause. For $B_Z > 0$ the reconnection site is poleward of the subsolar point. This explains why there was no erosion at the subsolar point of the dayside magnetopause. Instead a magnetic island forms there and the dayside reconnection rate becomes weaker. Reconnected flux is still convected into the tail where it reconnects and returns to the dayside.

We have not included an IMF B_Y or changes in the dynamic pressure in our calculations yet, so that we cannot directly compare our results with HST images in January, 2004 when the pressure enhancements associated with the CIRs reached Saturn [*Crary et al.,* 2005; *Badman et al.,* 2005]. In our calculations so far several patterns have emerged. First the largest energy flux and presumably the diffuse auroral emissions occur on the dawn side where flows are opposite to the solar wind-induced flow.

Second the strongest vortices and hence field-aligned currents also occur near dawn. This indicates that the strongest discrete aurorae also should be found near dawn.

4.4 Summary

We have used three dimensional magnetohydrodynamic simulations to investigate the influence of the interplanetary magnetic field (IMF) on the Kronian magnetosphere for cases with no IMF, northward and southward IMF. The subsolar magnetopause and bow shock positions are sensitive to changes in the solar wind dynamic pressure but insensitive to changes in the IMF. Without an IMF vortices were generated near dawn where the corotating flows and solar wind are opposite. For $B_Z < 0$ the vorticity results from the interaction of flows driven by cusp reconnection and corotation. For $B_Z > 0$ vortices were generated in the morning and evening where the flows from tail reconnection are opposite to the solar wind and corotation and the magnetic islands are formed at the dayside of magnetopause. We used the energy flux toward the ionosphere and upward field-aligned currents (FACs) as proxies for diffuse and discrete aurorae. Strong upward FACs extend to the morning sector when $B_Z > 0$. The strongest FACs are generated in the flow vortices.

Chapter 5

Conclusions

In this dissertation, we have studied the interaction of the solar wind and magnetospheric dynamics of rapidly rotating and giant planets such as Jupiter and Saturn. For Jupiter we have studied how the configuration of the magnetosphere responds under the lower solar wind dynamic pressures and what determines the periodic plasmoid ejections in the magnetotail (in Chapter 3). On the other hand, for Saturn we have investigated the effects of the IMF direction to the aurora brightness through the magnetospheric convection (in Chapter 4). In order to understand the complicated interaction of the solar wind and these planetary magnetospheres, we have performed global three dimensional MHD simulations. The conclusions of this dissertation are summarized as follows:

1. Jovian Magnetosphere

   First we have run the simulation of Jovian magnetosphere by setting the dynamic pressure to 0.090 nPa and it decreased three times until 0.011 nPa to investigate the effects of dynamic pressure on the magnetospheric configuration in the absence of an IMF. As results, the bow shock and magnetopause widely moved with the decreasing dynamic pressure. In addition, the cushion region which

is located between the magnetopause and the corotation boundary at dayside is dynamically increased under the lower dynamic pressure, and it is revealed that the configuration of Jovian magnetosphere becomes different state compared to cases with higher dynamic pressure.

Then we have simulated the magnetosphere for northward and southward IMF starting from the configuration with 0.011 nPa. Starting from the simulation with southward IMF we have examined a northward IMF of 0.105 nT simulation. In this simulation X/O pairs of neutral lines were launched tailward around 120 R_J with an average period of 34.3 hours. To investigate this peridic dynamics, we have run additional seven simulations with the changing both the dynamic pressure and the IMF strength. We found that the magnitude of IMF mostly controlls the location of tail reconnection and the solar wind dynamic pressure dominates the distance of corotation boundary. The position of the tail neutral line in turn determines how the reconnection generated flows interact with the rotating plasma sheet. For small pressures and IMF, tail reconnection becomes periodic. In these cases the neutral line forms far from the outer edge of the rotating plasma sheet. Flux tubes generated by tail reconnection can convect completely around Jupiter and return to the tail. When they reach the tail and accumulate there, the magnetic field become stretched and can reconnect. The new X/O pair forces the original X/O pair to move down the tail away from Jupiter. When the dynamic pressure and IMF are larger, the tail reconnection becomes steady. In some cases the flow from the reconnection reverses near the dawn magnetopause and returns tailward. If the reconnection driven flows are strong enough and the neutral line is near enough, the Jupiterward flow from the neutral line compresses the plasma sheet. In these cases the reconnected flux tubes rotate around Jupiter but exit along the dusk flank and do not contribute to

the reconnection multiple times.

2. Kronian Magnetosphere

To clarify the influence of the direction of IMF on the Kronian magnetosphere and aurora brightness, we have used a three dimensional MHD simulation. We have modeled the magnetosphere for a case with no IMF and for northward and southward IMF. The subsolar magnetopause and bow shock are insensitive to changes in the IMF. In the Y-direction the boundaries are farthest from Saturn for the case without IMF and farther for southward IMF than northward IMF. Flow vortices formed in the magnetotail for all three cases. They were confined to the inner magnetotail for northward IMF but were found throughout the tail for the southward and no IMF cases. For the no IMF case the vortices were generated in the morning sector where the rotating Kronian flows were opposite to the solar wind induced flows. For the southward IMF the vorticity results from the interaction of flow driven by high latitude reconnection and corotation. For northward IMF vortices were generated in the early morning and evening where the flows from reconnection in Saturn's tail were opposite to the solar wind induced flow. In this case the magnetic isalands are formed at the dayside of magnetopause. As mentioned above, it is clear that the Kronian magnetosphere tend to have the vortices and it is consistent with some observations results. In addition, we used the energy flux to the ionosphere and upward field-aligned currents as a proxy for diffuse and discrete auroral emissions respectively. For the no IMF case the energy flux is largest in the morning sector poleward of 75^o latitude consistent with HST observations during January 2004. With southward IMF the distribution of energy flux becomes more symmetric than that of the northward and no IMF cases. The energy flux in the polar cusp is dependent

on IMF orientation with larger energy flux for northward IMF. Strong upward field-aligned currents extend to the morning sector when the IMF is northward. Moreover, we found that the strongest field-aligned currents are generated in the flow vortices.

3. Future Works

In this dissertation, some of the complicated dynamics of Jovian and Kronian magnetosphere interacted with the solar wind become clear. However, our simulation model includes the plasma sources from the moon like Io and Enceladus but does not consider the variations and dynamics of those plasma sources. Io and Enceladus are the main plasma sources of the magnetosphere and those are possible enough that the variation of the plasma production affects the dynamics of global magnetospheres. The reason why we have not included the variation is that the Alfvén speed is very high near Jupiter and Saturn due to the intrinsic magnetic field then it becomes difficult to satisfy the Courant condition of numerical stability. To overcome the problem, one solution is to apply the Multi Scale grid (MS) method. Using MS method, the time and space resolutions are set independently to create another simulation box in the original simulation box. However MS method has not been applied in the space simulation because of the difficulty in transfer data from grid to grid with parallel computation. In addition we can not accurately treat the magnetosphere and ionosphere (M-I) coupling. To concretely analyse the M-I coupling, the ionospheric environment parameter such as conductivity must be included.

References

[1] Badman, S. V., E. J. Bunce, J. T. Clarke, S. W. H. Cowley, J.-C. Gérard, D. Grodent, S. E. Milan, Open flux estimates in Saturn's magnetosphere during the January 2004 Cassini-HST campaign, and implications for reconnection rates, *J. Geophys. Res., 110*, A11216, doi:10.1029/2005JA011240, 2005.

[2] Belcher, J. W., The low-energy plasma in the Jovian magnetosphere, In:Dessler, A. J. (Ed.), *Physics of the Jovian magnetosphere.* Cambridge University Press, New York, 1983.

[3] Bridge, H. S., et al., Plasma observations near Jupiter: initial results from Voyager 1, *Science 204*, 987, 1979a.

[4] Bridge, H. S., et al., Plasma observations near Jupiter: initial results from Voyager 2, *Science 206*, 972, 1979b.

[5] Bunce, E. J., S. W. H. Cowley, and S. E. Milan, Interplanetary magnetic field control of Saturn's polar cusp aurora, *Ann. Geophys., 23*, 1405, 2005.

[6] Bunce, E. J., S. W. H. Cowley, C. M. Jackman, J. T. Clarke, F. J. Crary, M. K. Dougherty, Cassini observations of the Interplanetary Medium Upstream of Saturn and their relation to the Hubble Space Telescope aurora data, *Adv. Space Res., 38*, 806, 2006.

[7] Cowley, S. W. H. and E. J. Bunce, Origin of the main auroral oval in Jupiter's coupled magnetosphere-ionosphere system, *Planet. Space Sci., 49*, 1067, 2001.

[8] Cowley, S. W. H., E. J. Bunce, T. S. Stallard, S. Miller, Jupiter's polar ionospheric flows: Theoretical interpretation, *Geophys. Res. Lett., 30*, 1220, doi:10.1029/2002GL016030, 2003.

[9] Cowley, S. W. H., E. J. Bunce and R. Prange, Saturn's polar ionospheric flows and their relation to the main auroral oval, *Ann. Geophys., 22*, 1379, 2004.

[10] Cowley, S. W. H., et al., Reconnection in a rotation-dominated magnetosphere and its relation to Saturn's auroral dynamics, *J. Geophys. Res., 110*, A02201, doi:10.1029/2004JA010796, 2005.

[11] Crary, F. J., et al., Solar wind dynamic pressure and electric field as the main factors controlling Saturn's aurorae, *Nature, 433*, 720, 2005.

[12] Dougherty, M. K., et al., Cassini magnetometer observations during Saturn orbit insertion, *Science, 307*, 1266. 1270, 2005.

[13] Fukazawa, K., T. Ogino, and R. J. Walker, Dynamics of the Jovian magnetosphere for northward interplanetary magnetic field (IMF), *Geophys. Res. Lett., 32*, doi:10.1029/2004GL021392, 2005.

[14] Fukazawa, K., T. Ogino and R. J. Walker, The Configuration and Dynamics of the Jovian Magnetosphere, *J. Geophys. Res., 111*, A10207, doi:10.1029/2006JA011874, 2006.

[15] Galopeau, P. H. M., P. Zarka, and D. Le Quéau, Source location of Saturn's kilometric radiation: The Kelvin-Helmholtz instability hypothesis, *J. Geophys. Res., 100*, 26,397, 1995.

[16] Hansen, K. C., A. J. Ridley, G. B. Hospodarsky, N. Achilleos, M. K. Dougherty, T. I. Gombosi, and G. Toth, A 3D Global MHD Simulation of Saturn's Magnetosphere at the time of Cassini approach, *Geophys. Res. Lett., 32*, doi:10.1029/2005GL022835, 2005.

[17] Hill, T.W., Inertial limit on corotation, *J. Geophys. Res., 84*, 6554, 1979.

[18] Hill, T. W., Dessler, A. J., Goertz, C. K., Magnetospheric models, In:Dessler, A. J. (Ed.), *Physics of the Jovian magnetosphere.* Cambridge University Press, New York, 1983.

[19] Hill, T.W., The jovian auroral oval, *J. Geophys. Res. 106*, 8101, 2001.

[20] Joy, S. P., M. G. Kivelson, R. J. Walker, K. K. Khurana, C. T. Russell, and T. Ogino, Probabilistic models of the Jovian magnetopause and bow shock locations, *J. Geophys. Res., 107,* A10, doi: 10. 1029/2001JA09146, 2002.

[21] Krupp, N., A. Lagg, S. Livi, B. Wilken, and J. Woch, Global flows of energetic ions in Jupiter's equatorial plane: First-order approximation, *J. Geophys. Res., 106*, 26017, 2001.

[22] Khurana, K. K., M. G. Kivelson, V. M. Vasyliunas, N. Krupp, J. Woch, A. Lagg, B. H. Mauk, W. S. Kurth, The Configuration of Jupiter's Magnetosphere, In:Bagenal, F., T. Dowling and W. McKinnon (Ed.), *Jupiter*, Cambridge University Press, New York, 2004.

[23] Kivilson, M. G., Does Enceladus Govern Magnetospheric Dynamics at Saturn?, *Science, 311*, 1391, 2006.

[24] Louarn, P., A. Roux, S. Perraut, W. Kurth, D. Gurnett, A study of the large-scale dynamics of the Jovian magnetosphere using the Galileo plasma wave experiment, *Geophys. Res. Lett., 25,* 2905, 1998.

[25] Louarn, P., A. Roux, S. Perraut, W. S. Kurth, D. A. Gurnett, A study of the Jovian "energetic magnetospheric events" observed by Galileo: role in the radial plasma transport, *J. Geophys. Res., 105,* 13073, 2000.

[26] Miyoshi, T., and K. Kusano, MHD Simulation of a Rapidly Rotating Magnetosphere Interacting with the External Plasma Flow, *Geophys. Res. Lett., 24*, 2627, 1997.

[27] Miyoshi, T., and K. Kusano, A Global MHD simulation of the Jovian magnetosphere interacting with/without the interplanetary magnetic field, *J. Geophys. Res., 106*, 10723, 2001.

[28] Ness, N. F., M. H. Acu, R. P. Lepping, J. E. P. Connerney, K. W. Behannon, L. F. Burlaga, and F. M. Neubauer, Magnetic field studies by Voyager 1: Preliminary results at Saturn, *Science, 212*, 211, 1981.

[29] Ogino, T., R. J. Walker, and M. Ashour-Abdalla, A global magnetohydrodynamic simulation of the magnetopause when the interplanetary magnetic field is northward, *IEEE Trans. Plasma Sci., 20*, 6817, 1992.

[30] Ogino, T., R. J. Walker, and M. Ashour-Abdalla, A global magnetohydrodynamic simulation of steady magnetospheric convection, *Proceedings of Second International Conference on Substorms*, 545, 1994

[31] Ogino, T., R.J. Walker, and M. Ashour-Abdalla. A Global Magentohydrodynamic Simulation of the Response of the Magneto-sphere to a Northward Tuning of the Interplanetary Magenetic Field, *J. Geophys. Res., 99*, 11,027, 1994.

[32] Ogino, T., R. J. Walker, and M. G. Kivelson, A global magnetohydrodynamic simulation of the Jovian magnetosphere, *J. Geophys. Res., 103*, 225, 1998.

[33] Phillips, J. L., Bame, S. J., Thomsen, M. F., Goldstein, B. E., Smith, E. J., Ulysses plasma observations in the Jovian magnetosphere, *J. Geophys. Res. 98,* 21,189, 1993.

[34] Reiner, M. J., M. L. Kaiser, M. D. Desch, Long-term behavior of Jovian bKOM and nKOM radio emissions observed during the Ulysses-Jupiter encounter, *Geophys. Res. Lett.*, 27, 297, 2000.

[35] Slavin, J. A., E. J. Smith, J. R. Spreiter, and S. S. Stahara, Solar wind flow about the outer planets -Gas dynamic modeling of the Jupiter and Saturn bow shocks, *J. Geophys. Res., 90*, 6275, 1985.

[36] Smith, E. J., Davis Jr., L., Jones, D. E., Jupiter's magnetic field and magnetosphere. In: *Gehrels,* T. (Ed.), Jupiter. University of Arizona Press, Tucson, 1976.

[37] Smith, E. J., Fillius, R. W., Wolfe, J. H., Compression of Jupiter's magnetosphere by the solar wind, *J. Geophys. Res. 83*, 4733, 1978.

[38] Southwood, D. J., and M. G. Kivelson, A new perspective concerning the influence of the solar wind on the Jovian magnetosphere, *J. Geophys. Res., 106*, A4, 6123, 2001.

[39] Stallard, T. S., S. Miller, S. W. H. Cowley, E. J. Bunce, Jupiter's polar ionospheric flows: Measured intensity and velocity variations poleward of the main auroral oval, *Geophys. Res. Lett., 30*, 1221, doi:10.1029/2002GL016031, 2003.

[40] Tokar, R. L., et al., The Interaction of the Atmosphere of Enceladus with Saturn's Plasma, *Science, 311*, 1409, 2006.

[41] Vasyliunas, V. M., Plasma distribution and flow, In:Dessler, A. J. (Ed.), *Physics of the Jovian magnetosphere*, Cambridge University Press, New York, 1983.

[42] Walker, R. J., T. Ogino, J. R. Raeder and M. Ashour-Abdalla, A global magnetohydrodynamic simulation of the magnetosphere when the interplanetary magnetic field is southward: The onset of magnetotail reconnection, *J. Geophys. Res., 98*, 17235, 1993.

[43] Walker, R. J., T. Ogino and M. G. Kivelson, Magnetohydrodynamic simulation of the effect of the solar wind on the Jovian magnetosphere, *Planet. Space. Sci., 49*, 237, 2001.

[44] Walker, R. J. and T. Ogino, A simulation study of currents in the Jovian magnetosphere, *Planet. Space. Sci., 51*, 295, 2003.

[45] Walker, R. J., S. P. Joy, M. G. Kivelson, K. Khurana, T. Ogino and K. Fukazawa, The locations and shapes of Jupiter's bow shock and magnetopause, The Physics of Collisionless Shocks, G. Li, G. P. Zank, and C. T. Russell, eds., *AIP Conference Proceedings, 781,* 95-108, 2005.

[46] Watanabe, K., and T. Sato, Global simulation of the solar wind-magnetosphere interaction: The importance of its numerical validity, *J. Geophys. Res., 95*, 75, 1990.

[47] Woch, J. N. Krupp, and A. Lagg, Particle bursts in the Jovian magnetosphere: Evidence for a near-Jupiter neutral line, *Geophys. Res. Lett., 29,* 10.1029/2001GL014080, 2002.

Papers published in connection with the present dissertation

- Fukazawa, K., T. Ogino, and R. J. Walker, Dynamics of the Jovian magnetosphere for northward interplanetary magnetic field (IMF), *Geophys. Res. Lett., 32*, doi:10.1029/2004GL021392, 2005.

- Walker, R. J., S. P. Joy, M. G. Kivelson, K. Khurana, T. Ogino and K. Fukazawa, The locations and shapes of Jupiter's bow shock and magnetopause, The Physics of Collisionless Shocks, G. Li, G. P. Zank, and C. T. Russell, eds., *AIP Conference Proceedings, 781,* 95-108, 2005.

- Fukazawa, K., T. Ogino and R. J. Walker, The Configuration and Dynamics of the Jovian Magnetosphere, *J. Geophys. Res., 111*, A10207, doi:10.1029/2006JA011874, 2006.

- Fukazawa, K., S. Ogi, T. Ogino, and R. J. Walker, Magnetospheric Convection at Saturn as a Function of IMF B_Z, *Geophys. Res. Lett., 34*, L01105, doi:10.1029/2006GL028373, 2007.